國 立 交 通 大 學

工學院半導體材料與製程設備學程

碩 士 論 文

ATV 被動式懸吊參數最佳化設計

Optimization design of passive suspension parameters for ATV

研 究 生：王學磊

指導教授：成維華　教授

中華民國九十七年七月

ATV 被動式懸吊參數最佳化設計

Optimization design of passive suspension parameters for ATV

研　　究　　生：王學磊　　Student：Hsueh-Lei Wang

指　導　教　授：成維華 博士　　Advisor：Dr.Wei-Hua Chieng

國 立 交 通 大 學

工學院半導體材料與製程設備學程

碩 士 論 文

A thesis

Submitted to Master Degree Program of Semiconductor Material and Processing Equipment

College of Engineering

National Chiao Tung University

in partial fulfillment of the requirements

for the degree of

Master of Science

in

Master Degree Program of Semiconductor Material and Processing Equipment

July 2008

Hsinchu, Taiwan, Republic of China

中華民國九十七年七月

ATV 被動式懸吊參數最佳化設計

研究生:王學磊　　指導教授:成維華 教授

國立交通大學工學院 半導體材料與製程設備學程 碩士班

摘　　要

ATV(All-Terrain Vehicle)為全地形車的簡稱,也可稱為沙灘越野車;從 1950s 年代開始發展至今，ATV 分為運動以及多用途兩大類。隨著人們對於戶外運動及娛樂的意識興起，由其在近期的極限運動中，使用 ATV 來進行沙漠、爬山及冰上等越野競賽；所以越野路面的震動情況，對於駕駛人員而言，一個很好的避震懸吊器可以讓駕駛人員獲得更好的舒適度及改善車輛的偏移。

本文主旨是利用基因演算法之全域最佳化方法，計算出最適合的被動式懸吊參數值後進行模擬；再利用六軸平台，以事先取得不同行駛路面之資訊，作動態分析與速度、加速度的量測；量測結果與先前基因演算法之全域最佳化方法計算出來的被動式懸吊參數比較，進而找出 ATV 最佳的被動式懸吊參數。

關鍵字：全地形車、基因演算法、被動式懸吊、動態分析。

Optimization design of passive suspension parameters for ATV

Student: Hsueh-Lei Wang Advisor: Dr. Wei-Hua Chieng

Master Degree Program of Semiconductor Material and Processing Equipment
College of Engineering
National Chiao Tung University

Abstract

The ATV is abbreviation of all-terrain vehicle or called the vehicle of off-road. Since 1950s, ATV were developed up to now and models continue today to be divided into the sport and utility markets. Following the raising of tendency toward outdoor exercise and recreation, in near future, extreme sport types of ATV were used on kinds of terrains, such as desert racing, hill climbing, ice racing etc. The vibration due to the rough road condition makes the passenger feel uncomfortable and a well adjusted suspension system will improve the car handling and more comfortable for passenger.

The objective of this paper is using global optimization method of the Genetic Algorithm, calculated and simulated optimize of passive suspension parameters for ATV. We are using Stewart platform and pre-obtained road profiles, measure and dynamic analysis of ATV to travel on off-road. The results are compare optimization of passive suspension parameters. Finding out the parameters of the ATV suspension optimized value.

Keywords: ATV, genetic algorithm, passive suspension, dynamic analysis.

誌　　謝

回顧在交大的時光，承蒙恩師 成維華 教授指導，不論在生活上的關懷及論文研究的悉心指導，讓弟子在工作及求學路上有更好的思維與想法，並且指引弟子人生方向，使弟子如沐春風、獲益良多；論文審查方面，感謝口試委員 鄭時龍 博士與 廖俊旭 博士對論文的指正與寶貴建議，以及領航動感科技(股)公司提供實驗之模擬器平台，使學生能順利完成論文，也讓研究成果能夠更趨完善。

在學期間，特別感謝實驗室 秉霖、嘉豐 學長提供協助及指正，讓我受益匪淺；也要感謝 偉鈞、侯兄、明欣、建成、曹兄、星雲、富源、強哥、文彬、小賴、洋豪 同學在學業上的相互扶持，以及安鎮、志隆、之皓、文祥、冠今 同學的幫助；感謝專班 雅聿、雅玲 小姐以及公司工作伙伴們；因為有了你們，讓我順利完成學業。

最後要感謝我的父母，沒有你們的養育及栽培，就沒有今日的我；以及女友 慕青，在生活上給我最大的支持與鼓勵，得以全心投入學習及研究，完成自己的理想與目標；謹將本論文獻給我的家人們，在此由衷地感謝。

王學磊 謹誌

中華民國九十七年七月

Contents

List of Tables

List of Figures

Nomenclature

k	: spring coefficient
c	: damping coefficient
l	: length of ATV model
w	: width of ATV model
O	: center-of-gravity position of ATV model
J	: jerk(rate of change for acceleration)
a_w	: the frequency weighted acceleration data
T_s	: measured time
N	: number of points
$\vec{Z}_A$	: the road profile data inputs to the A wheel suspension
$\vec{Z}_B$	: the road profile data inputs to the B wheel suspension
$\vec{Z}_C$	: the road profile data inputs to the C wheel suspension
$\vec{Z}_D$	: the road profile data inputs to the D wheel suspension
$\vec{Z}$	: the vertical displacement along the z-axis of ATV
$\vec{Z}_0$	: the origin point of local reference
$\ddot{z}$	: vertical acceleration of ATV
R_x	: rotation matrix of roll
R_y	: rotation matrix of pitch
R_v	: rotation matrix of ATV
α	: roll angle of ATV
β	: pitch angle of ATV
γ	: yaw angle of ATV
$\dot{\alpha}$	: roll angle velocity of ATV
$\dot{\beta}$	: pitch angle velocity of ATV
N_{pop}	: size of initial population

Chapter 1 Introduction

1.1 Introduction and development of ATV

The ATV is abbreviation of all-terrain vehicle or all ground transport carrier. The ATV is usually used to describe any of a number of small open motorized buggies and tricycles designed for off-road use. About the ATV has well the adaptability going on any different landform. Generally, the ATV is called the vehicle of off-road or the vehicle of beach.

The first ATV was made during 1950s. Originally, the vehicle structure of 6-wheels comes to replace vehicle structure of 4-wheels. Honda Corporation made the first 3-wheels ATV in 1970 and Suzuki Corporation development first 4-wheels ATV is 1983. Afterward ATV prototype of 3 or 4-wheels models were developed, models continue today to be divided into the sport and utility markets [1].

The ATV is usually 3 or 4-wheels structure and 6 or 8-wheels for special application. Such as the armored vehicle of military used. The American National Standards Institute (ANSI) defines an ATV as a vehicle that travels on low pressure tires, with one seat that is straddled by the operator, and with handlebars for steering control. Extensively use to the outdoor exercise and amusement now [1].

Following the raising of tendency toward outdoor exercise and Recreation, the characteristic of sport ATV models must have light weight, high power, low center of gravity and good suspension. Figure 1.1 illustrated a sport ATV made by Honda (Honda TRX250EX Sport ATV). Sport models are built with performance, rather than utility. Sport models

are generally small, light, two wheel drive vehicles which accelerate quickly, have a manual transmission, and run at speeds up to 90 miles per hour [1]. In near future, extreme sport types of ATV were used on kinds of terrains, such as desert racing, hill climbing, ice racing etc. The vibration due to the rough road condition makes the passenger feel uncomfortable and a well adjusted suspension system will improve the car handling and more comfortable for passenger [1].

1.2 Literature review

The classifications of suspension have 3 types, master types are active suspension, semi-active suspension and passive suspension. Compare these three kinds of forms, characteristic of passive suspension is cheaper and easier to adjust and repair. Therefore, Passive suspension system is popularly used on ATV, including automotive. One degree-of-freedom or two degree-of-freedom quarter-car models are commonly employed in many areas of the automotive industry, including optimization of suspensions of vehicles [2]. A design optimization of quarter-car models with passive suspensions under random road excitation was proposed [3]. Evaluation of the vehicle performance is based on examination of three response quantities, that is, the maximum absolute acceleration of the passengers, the distance between the wheel subsystem and the car-body and the force developed between the wheel and the ground [1].

With evaluations of the vehicle comfort are usually used to optimize vehicle suspension. A typical measure of comfort has the form shown in equation 1-1[4].

$$J = \int_0^t \ddot{z}(t)^2 dt \tag{1-1}$$

Car-body travel distance and velocity, as in equations 1-2 and 1-3 below, are also used [5].

$$J = \int_0^t z(t)^2 dt \tag{1-2}$$

$$J = \int_0^t \dot{z}(t) dt \tag{1-3}$$

The jerk (rate of change of acceleration) can also be used as a measure of comfort, use equation 1-4 [6]

$$J = \int_0^t \dddot{z}(t)^2 dt \tag{1-4}$$

Besides, the measure of comfort, RMS (root mean square) is basic method of estimate for vibration, ISO 2631-1(1997) used this method and shown in equation 1-5. [13][23]

$$RMS = \left[\frac{1}{N} \sum_{n=1}^{N} a_w^2 \right]^{1/2} \tag{1-5}$$

And VDV (Vibration Does Value) uses fourth power vibration dose method shown in equation 1-6 [7]. [23]

$$VDV = \left[\frac{T_s}{N} \sum_{n=1}^{N} a_w^4 \right]^{1/4} \tag{1-6}$$

In [8], equation 1-4 was used as the measure of comfort and evolutionary algorithm was applied to the optimization of the system parameters. An optimal design for passive suspension of a light rail Rapid Transit also using evolutionary algorithm has been issued [9]. A systematic and effective optimization scheme for the design of vehicle passive suspension system was proposed [10] [11].

Equation 1-5 and 1-6 are chosen as one of the measures of comfort

because it's more sensitive of acceleration and a full-car model is used to provide a three degree-of-freedom model of ATV [1]. The global optimization algorithm, Genetic algorithm (or evolutionary algorithm), is selected to optimize the passive suspension parameters [1].

1.3 Motives and objectives

ATV is usually driver on off-road or rough terrains. Therefore, about the driver or rider of ATV to travel on off-road or rough terrains, reduce vibration to make the passenger feel uncomfortable is very important. In order to maintain the stability and improve the driving comfort, an effective method for designing suspension parameters is needed [1].

Figure 1.2 is passive suspension systems structure, the parameter such as spring coefficient k and damping coefficient c. According to the Genetic Algorithm and optimize of passive suspension parameters (spring coefficient k and damping coefficient c) for ATV, simulation and analysis ATV to travel on off-road using road profile data of the game.

Therefore, according to the above, this research is measure and dynamic analysis of ATV to travel on off-road using road profile data of the game and compare optimization of passive suspension parameters (spring coefficient k and damping coefficient c). Finding out the parameters of the ATV suspension optimize value.

Chapter 2 Dynamic model and definition of ATV passive suspension system

2.1 Historical review

Whole body vibration (WBV) is the mechanical vibration or shock transmitted to the body as a whole. It is usually due to the vibration of the body surface supporting [12]. The effects of vibration could be subdivided into three main topics, namely (a) interference with comfort, (b) interference with activities and (c) interference with health. Each criterion has different conditions and limits associated with it.

Most researchers indicated that seated humans or drivers have a vertical vibration natural frequency approximate to 4~6Hz and a horizontal vibration natural frequency approximate to 1~2Hz [12] [17].In this frequency ranges the seat motion is most easily transmitted to the upper parts of the body and is not just confined to the area of the body close to the source of vibration [12] [17].

WBV exposures are to be determined separately for the three axes in accordance with ISO 2631-1:1997. But up to date the literature review explained, prove and quantization the vibration value of seated humans with VDV measurements [14]. The VDV is abbreviation of Vibration Dose Value.

VDV is based on the fourth power of acceleration and is therefore more sensitive to shocks compared to the RMS (root mean square) magnitude (ISO 2631-1:1997). The general formula for VDV is

$$VDV_z = \left[\frac{T_s}{N} \sum_{n=1}^{N} a_w^4 \right]^{1/4} \tag{2-1}$$

with T_s the measured time, N the number of points and a_w the frequency weighted acceleration data. This parameter is time dependent and gives an objective measure of the amount of vibrations a person had to experience with a certain period [1]. There VDV_z is z-axis vibration target ($m/s^{1.75}$).

VDV is used as an index of vertical vibration. It is enough that generally adopt the vibration of ISO 2631-1 method RMS (root mean square). Besides, RMS is basic method of estimate for vibration, ISO 2631-1(1997) used this method, acceleration unit is m/s^2 and rotation acceleration unit is rad/s. The general form for RMS acceleration is

$$RMS = \left[\frac{1}{N} \sum_{n=1}^{N} a_w^2 \right]^{1/2} \tag{2-2}$$

with N the number of points and a_w the frequency weighted acceleration data.

The RMS angular velocity is used in this paper as the index of rotation vibration. The general form for RMS angular velocity is

$$J_\alpha = \left[\frac{1}{N} \sum_{n=1}^{N} \dot{\alpha}_w^2 \right]^{1/2} \tag{2-3}$$

$$J_\beta = \left[\frac{1}{N} \sum_{n=1}^{N} \dot{\beta}_w^2 \right]^{1/2} \tag{2-4}$$

with N the number of points and $\dot{\alpha}$, $\dot{\beta}$ the frequency weighted acceleration data [1]. There J_α is roll angular rotation target (rad/s) and J_β is pitch angular rotation target (rad/s). The reason of frequency weighting is that human body is more sensitive to certain vibration frequency [1].

In order to let us simulation and measurement result ($\ddot{z}, \dot{\alpha}, \dot{\beta}$) can be closer to the frequency of the human body experiences in fact. We referenced the frequency weighting curves diagram shown in Figure 2.1 and 2.2 [17] [23]. A couple of weightings curves (filters) are specified by ISO 2631:1997 depending on the orientation of the person and the direction of vibration. The black line represents the W_k weighting curve and the blue one represents the W_e weighting curve. The lateral axis is frequency represented in log scale and the vertical axis is magnitude represented in log scale, too. For a seated person the W_k curve is used to weight the frequency contribution for vertical vibrations and the W_e curve is used to weigh the frequency contribution for rotation vibrations [13].

Assessments are made independently in each direction. Figure 2.3 shows which weighting curve should be applied to which axis [17] [25]. For rotation vibration, the weighting curve is W_e and for vertical vibration, the weighting curve is W_k. A second order shaped curve of the form

$$H_k(s) = \frac{50s + 500}{s^2 + 50s + 1200} \tag{2-5}$$

has been used in [14, 15] to approximate the ISO weighting curve W_k and shown in Figure 2.4. Another second order shaped curve of the form

$$H_e(s) = \frac{9s + 20}{s^2 + 10s + 40} \tag{2-6}$$

has been used to approximate the ISO weighting curve W_e and shown in Figure 2.5.

Finally, Simulation and measurement results ($\ddot{z}, \dot{\alpha}, \dot{\beta}$) multiplication frequency weighting values(W_k, W_e, W_e) , we can get be closer to the frequency of the human body experiences in fact.

2.2 Derive of dynamic equations [1]

About an integral model of ATV is illustrated in Figure 2.6. We consider here has three degree-of-freedom including vertical displacement of center-of-gravity position, roll and pitch angles. A segment and D segment are the front wheels of two passive suspensions, B segment and C segment are the rear wheels of two passive suspensions. As to ATV, O point is center-of-gravity position. $\overline{Z}_A, \overline{Z}_B, \overline{Z}_C, \overline{Z}_D$ are the road profile data inputs to the four suspensions of ATV, respectively. $\overline{Z}$ is the vertical displacement along the z-axis of ATV. When vehicle (ATV) body rotated in the inertial, the included angles are roll, pitch and yaw angles, with notations α, β and γ respectively, there angles are called the Euler angles. The rotate angle (roll, pitch angles (α, β)) are according to right-hand rule. Here we assume γ is very small and can be neglected when driving alone a straight lane. Therefore, the rotation matrix of the vehicle can be represented as follow.

Because the rotation matrix contact with vertical axis, so θ_z=0.

$$R_v(\theta_x,\theta_y,\theta_z) = R_v(\theta_x,\theta_y) = (R_x,R_y)^{-1} = (R_y^{-1} * R_x^{-1}) = \begin{bmatrix} \cos\beta & \sin\alpha\sin\beta & \cos\alpha\sin\beta \\ 0 & \cos\alpha & -\sin\alpha \\ -\sin\beta & \sin\alpha\cos\beta & \cos\alpha\cos\beta \end{bmatrix} \quad (2\text{-}7)$$

R_x and R_y are shown as follows

Roll axis: $$R_x(\alpha) = \begin{bmatrix} 1 & 0 & 0 \\ 0 & \cos\alpha & \sin\alpha \\ 0 & -\sin\alpha & \cos\alpha \end{bmatrix}$$

Pitch axis: $$R_y(\beta)=\begin{bmatrix}\cos\beta & 0 & -\sin\beta\\ 0 & 1 & 0\\ \sin\beta & 0 & \cos\beta\end{bmatrix} \tag{2-8}$$

After the simplification rotation matrix R_v, according to the above, the rotated vectors from O to each suspension (A, B, C, D point) can be represented as follows

$$\overrightarrow{OA}' = R_v(\theta_x,\theta_y)\cdot\overrightarrow{OA}+(\vec{Z}-\vec{Z_0}) = \begin{bmatrix}\frac{\ell}{2}\cos\beta+\frac{w}{2}\sin\alpha\sin\beta\\ \frac{w}{2}\cos\alpha\\ -\frac{\ell}{2}\sin\beta+\frac{w}{2}\sin\alpha\cos\beta\end{bmatrix}+(\vec{Z}-\vec{Z_0})$$

$$\overrightarrow{OB}' = R_v(\theta_x,\theta_y)\cdot\overrightarrow{OB}+(\vec{Z}-\vec{Z_0}) = \begin{bmatrix}-\frac{\ell}{2}\cos\beta+\frac{w}{2}\sin\alpha\sin\beta\\ \frac{w}{2}\cos\alpha\\ \frac{\ell}{2}\sin\beta+\frac{w}{2}\sin\alpha\cos\beta\end{bmatrix}+(\vec{Z}-\vec{Z_0})$$

$$\overrightarrow{OC}' = R_v(\theta_x,\theta_y)\cdot\overrightarrow{OC}+(\vec{Z}-\vec{Z_0}) = \begin{bmatrix}-\frac{\ell}{2}\cos\beta-\frac{w}{2}\sin\alpha\sin\beta\\ -\frac{w}{2}\cos\alpha\\ \frac{\ell}{2}\sin\beta-\frac{w}{2}\sin\alpha\cos\beta\end{bmatrix}+(\vec{Z}-\vec{Z_0})$$

$$\overrightarrow{OD}' = R_v(\theta_x,\theta_y)\cdot\overrightarrow{OD}+(\vec{Z}-\vec{Z_0}) = \begin{bmatrix}\frac{\ell}{2}\cos\beta-\frac{w}{2}\sin\alpha\sin\beta\\ -\frac{w}{2}\cos\alpha\\ -\frac{\ell}{2}\sin\beta-\frac{w}{2}\sin\alpha\cos\beta\end{bmatrix}+(\vec{Z}-\vec{Z_0}) \tag{2-9}$$

About the model of ATV, $\vec{Z}_0$ is the origin point of local reference, and $(\vec{Z}-\vec{Z_0})$ is vertical displacement change. Then we can derive the vertical displacement of each suspension, and we assumed α and β

were small and furthermore we applied linearization.

$$\overrightarrow{d_A} = \overrightarrow{OA}' - \overrightarrow{OA} = \begin{bmatrix} \frac{\ell}{2}(\cos\beta - 1) + \frac{w}{2}\sin\alpha\sin\beta \\ \frac{w}{2}(\cos\alpha - 1) \\ -\frac{\ell}{2}\sin\beta + \frac{w}{2}\sin\alpha\cos\beta \end{bmatrix} + (\vec{Z} - \vec{Z}_0) \simeq (-\frac{\ell}{2}\beta + \frac{w}{2}\alpha + z)\begin{bmatrix} 0 \\ 0 \\ 1 \end{bmatrix}$$

$$\overrightarrow{d_B} = \overrightarrow{OB}' - \overrightarrow{OB} = \begin{bmatrix} -\frac{\ell}{2}(\cos\beta - 1) + \frac{w}{2}\sin\alpha\sin\beta \\ \frac{w}{2}(\cos\alpha - 1) \\ \frac{\ell}{2}\sin\beta + \frac{w}{2}\sin\alpha\cos\beta \end{bmatrix} + (\vec{Z} - \vec{Z}_0) \simeq (\frac{\ell}{2}\beta + \frac{w}{2}\alpha + z)\begin{bmatrix} 0 \\ 0 \\ 1 \end{bmatrix}$$

$$\overrightarrow{d_C} = \overrightarrow{OC}' - \overrightarrow{OC} = \begin{bmatrix} -\frac{\ell}{2}(\cos\beta - 1) - \frac{w}{2}\sin\alpha\sin\beta \\ -\frac{w}{2}(\cos\alpha - 1) \\ \frac{\ell}{2}\sin\beta - \frac{w}{2}\sin\alpha\cos\beta \end{bmatrix} + (\vec{Z} - \vec{Z}_0) \simeq (\frac{\ell}{2}\beta - \frac{w}{2}\alpha + z)\begin{bmatrix} 0 \\ 0 \\ 1 \end{bmatrix}$$

$$\overrightarrow{d_D} = \overrightarrow{OD}' - \overrightarrow{OD} = \begin{bmatrix} \frac{\ell}{2}(\cos\beta - 1) - \frac{w}{2}\sin\alpha\sin\beta \\ -\frac{w}{2}(\cos\alpha - 1) \\ -\frac{\ell}{2}\sin\beta - \frac{w}{2}\sin\alpha\cos\beta \end{bmatrix} + (\vec{Z} - \vec{Z}_0) \simeq (-\frac{\ell}{2}\beta - \frac{w}{2}\alpha + z)\begin{bmatrix} 0 \\ 0 \\ 1 \end{bmatrix}$$

(2-10)

We assume

$$\vec{Z}_0 = \begin{bmatrix} 0 \\ 0 \\ 0 \end{bmatrix} \qquad (2\text{-}11)$$

To get the net vertical displacement value of each suspension, we subtract the road input form ($\vec{Z}_A, \vec{Z}_B, \vec{Z}_C, \vec{Z}_D$ segment) vertical displacement of each suspension.

$$\overrightarrow{d_A}-\overrightarrow{z_A}=\left(-\frac{\ell}{2}\beta+\frac{w}{2}\alpha+z-z_A\right)\begin{bmatrix}0\\0\\1\end{bmatrix},\dot{\overrightarrow{d_A}}-\dot{\overrightarrow{z_A}}=\left(-\frac{\ell}{2}\dot{\beta}+\frac{w}{2}\dot{\alpha}+\dot{z}-\dot{z}_A\right)\begin{bmatrix}0\\0\\1\end{bmatrix}$$

$$\overrightarrow{d_B}-\overrightarrow{z_B}=\left(\frac{\ell}{2}\beta+\frac{w}{2}\alpha+z-z_B\right)\begin{bmatrix}0\\0\\1\end{bmatrix},\dot{\overrightarrow{d_B}}-\dot{\overrightarrow{z_B}}=\left(\frac{\ell}{2}\dot{\beta}+\frac{w}{2}\dot{\alpha}+\dot{z}-\dot{z}_B\right)\begin{bmatrix}0\\0\\1\end{bmatrix}$$

$$\overrightarrow{d_C}-\overrightarrow{z_C}=\left(\frac{\ell}{2}\beta-\frac{w}{2}\alpha+z-z_C\right)\begin{bmatrix}0\\0\\1\end{bmatrix},\dot{\overrightarrow{d_C}}-\dot{\overrightarrow{z_C}}=\left(\frac{\ell}{2}\dot{\beta}-\frac{w}{2}\dot{\alpha}+\dot{z}-\dot{z}_C\right)\begin{bmatrix}0\\0\\1\end{bmatrix}$$

$$\overrightarrow{d_D}-\overrightarrow{z_D}=\left(-\frac{\ell}{2}\beta-\frac{w}{2}\alpha+z-z_D\right)\begin{bmatrix}0\\0\\1\end{bmatrix},\dot{\overrightarrow{d_D}}-\dot{\overrightarrow{z_D}}=\left(-\frac{\ell}{2}\dot{\beta}-\frac{w}{2}\dot{\alpha}+\dot{z}-\dot{z}_D\right)\begin{bmatrix}0\\0\\1\end{bmatrix}$$

(2-12)

We infer the suspension compression distance and the speed. With the net vertical displacement value of each suspension and its first derivative, we derive the equations of motion from applying Lagrangian Dynamics.

$$T=\frac{1}{2}m\dot{\vec{Z}}^2+\frac{1}{2}I_x\dot{\vec{\theta}}_x^2+\frac{1}{2}I_y\dot{\vec{\theta}}_y^2$$

$$V=mg(\vec{Z}-\vec{Z}_0)+\frac{1}{2}k_A(\vec{d}_A-\vec{z}_A)^2+\frac{1}{2}k_B(\vec{d}_B-\vec{z}_B)^2+\frac{1}{2}k_C(\vec{d}_C-\vec{z}_C)^2+\frac{1}{2}k_D(\vec{d}_D-\vec{z}_D)^2$$

(2-13)

Here T represents the kinetic energy and V represents the potential energy of the system. We assume the front wheels of two passive suspensions *k*(spring coefficient) and *c*(damping coefficient) are equal, and the rear wheels of two passive suspensions *k*(spring coefficient) and *c*(damping coefficient) are equal.

$$\begin{cases} k_A = k_D = k_f \\ k_B = k_C = k_r \\ c_A = c_D = c_f \\ c_B = c_C = c_r \end{cases} \tag{2-14}$$

Then we have

$$T = \frac{1}{2} m \dot{\bar{Z}}^2 + \frac{1}{2} I_x \dot{\bar{\theta}}_x^2 + \frac{1}{2} I_y \dot{\bar{\theta}}_y^2$$

$$V = mg(\bar{Z} - \bar{Z}_0) + \frac{1}{2} k_f ((\bar{d}_A - \bar{z}_A)^2 + (\bar{d}_D - \bar{z}_D)^2) + \frac{1}{2} k_r ((\bar{d}_B - \bar{z}_B)^2 + (\bar{d}_C - \bar{z}_C)^2)$$

$$L = T - V \tag{2-15}$$

and the generalized forces can be derived as follows.

$$\begin{aligned} \bar{Q}_Z &= -c_A(\dot{\bar{d}}_A - \dot{\bar{z}}_A) - c_B(\dot{\bar{d}}_B - \dot{\bar{z}}_B) - c_C(\dot{\bar{d}}_C - \dot{\bar{z}}_C) - c_D(\dot{\bar{d}}_D - \dot{\bar{z}}_D) \\ &= -c_f(\dot{\bar{d}}_A + \dot{\bar{d}}_D - \dot{\bar{z}}_A - \dot{\bar{z}}_D) - c_r(\dot{\bar{d}}_B + \dot{\bar{d}}_C - \dot{\bar{z}}_B - \dot{\bar{z}}_C) \\ \bar{Q}_{\theta_x} &= \frac{w}{2}[-c_A(\dot{\bar{d}}_A - \dot{\bar{z}}_A) - c_B(\dot{\bar{d}}_B - \dot{\bar{z}}_B)] - \frac{w}{2}[-c_C(\dot{\bar{d}}_C - \dot{\bar{z}}_C) - c_D(\dot{\bar{d}}_D - \dot{\bar{z}}_D)] \\ &= -\frac{w}{2}[c_f(\dot{\bar{d}}_A - \dot{\bar{z}}_A - \dot{\bar{d}}_D + \dot{\bar{z}}_D) + c_r(\dot{\bar{d}}_B - \dot{\bar{z}}_B - \dot{\bar{d}}_C + \dot{\bar{z}}_C)] \\ \bar{Q}_{\theta_y} &= \frac{\ell}{2}[-c_B(\dot{\bar{d}}_B - \dot{\bar{z}}_B) - c_C(\dot{\bar{d}}_C - \dot{\bar{z}}_C)] - \frac{\ell}{2}[-c_D(\dot{\bar{d}}_D - \dot{\bar{z}}_D) - c_A(\dot{\bar{d}}_A - \dot{\bar{z}}_A)] \\ &= -\frac{\ell}{2}[-c_f(\dot{\bar{d}}_D - \dot{\bar{z}}_D + \dot{\bar{d}}_A - \dot{\bar{z}}_A) + c_r(\dot{\bar{d}}_B - \dot{\bar{z}}_B + \dot{\bar{d}}_C - \dot{\bar{z}}_C)] \end{aligned} \tag{2-16}$$

Substituting (2-15) and (2-16) into the Lagrange's equation as follows.

$$\frac{d}{dt}\left(\frac{\partial L}{\partial \dot{\bar{Z}}}\right) - \frac{\partial L}{\partial \bar{Z}} = \bar{Q}_Z$$

$$\frac{d}{dt}\left(\frac{\partial L}{\partial \dot{\bar{\theta}}_x}\right) - \frac{\partial L}{\partial \bar{\theta}_x} = \bar{Q}_{\theta_x}$$

$$\frac{d}{dt}\left(\frac{\partial L}{\partial \dot{\bar{\theta}}_y}\right) - \frac{\partial L}{\partial \bar{\theta}_y} = \bar{Q}_{\theta_y} \tag{2-17}$$

We obtained the three equations of motion of the ATV.

$$m\ddot{z} + mg + k_f(-\ell\beta + 2z - z_A - z_D) + k_r(\ell\beta + 2z - z_B - z_C) + c_f(-\ell\dot{\beta} + 2\dot{z} - \dot{z}_A - \dot{z}_D) + c_r(\ell\dot{\beta} + 2\dot{z} - \dot{z}_B - \dot{z}_C) = 0 \quad (2\text{-}18)$$

$$I_x\ddot{\alpha} + \frac{w}{2}[k_f(w\alpha - z_A + z_D) + k_r(w\alpha - z_B + z_C)] + \frac{w}{2}[c_f(w\dot{\alpha} - \dot{z}_A + \dot{z}_D) + c_r(w\dot{\alpha} - \dot{z}_B + \dot{z}_C)] = 0 \quad (2\text{-}19)$$

$$I_y\ddot{\beta} + \frac{\ell}{2}[-k_f(-\ell\beta + 2z - z_A - z_D) + k_r(\ell\beta + 2z - z_B - z_C)] + \frac{\ell}{2}[-c_f(-\ell\dot{\beta} + 2\dot{z} - \dot{z}_A - \dot{z}_D) + c_r(\ell\dot{\beta} + 2\dot{z} - \dot{z}_B - \dot{z}_C)] = 0 \quad (2\text{-}20)$$

The above equations of motion (2-18), (2-19), (2-20) can be rearrange as follows

$$[M]\{\ddot{q}\} + [C]\{\dot{q}\} + [K]\{q\} = [r] \quad ,where\ q = \begin{bmatrix} z \\ \alpha \\ \beta \end{bmatrix} \quad (2\text{-}21)$$

Finally, the state-space form of the system is written as follows

$$\begin{bmatrix} \dot{q} \\ \ddot{q} \end{bmatrix} = \begin{bmatrix} 0 & I \\ -M^{-1}K & -M^{-1}C \end{bmatrix} \begin{bmatrix} q \\ \dot{q} \end{bmatrix} + \begin{bmatrix} 0 \\ M^{-1} \end{bmatrix} r(t)$$
$$\begin{bmatrix} q \\ \dot{q} \\ \ddot{q} \end{bmatrix} = \begin{bmatrix} I & 0 \\ 0 & I \\ -M^{-1}K & -M^{-1}C \end{bmatrix} \begin{bmatrix} q \\ \dot{q} \end{bmatrix} + \begin{bmatrix} 0 \\ 0 \\ M^{-1} \end{bmatrix} r(t) \quad (2\text{-}22)$$

where

$$M = \begin{bmatrix} m & 0 & 0 \\ 0 & I_x & 0 \\ 0 & 0 & I_y \end{bmatrix} \quad (2\text{-}23)$$

$$C = \begin{bmatrix} 2(cf+cr) & 0 & \ell(-cf+cr) \\ 0 & \frac{w^2}{2}(cf+cr) & 0 \\ \ell(-cf+cr) & 0 & \frac{\ell^2}{2}(cf+cr) \end{bmatrix} \tag{2-24}$$

$$K = \begin{bmatrix} 2(kf+kr) & 0 & \ell(-kf+kr) \\ 0 & \frac{w^2}{2}(kf+kr) & 0 \\ \ell(-kf+kr) & 0 & \frac{\ell^2}{2}(kf+kr) \end{bmatrix} \tag{2-25}$$

2.3 Definition of cost function

The spring coefficient k and damping coefficient c of passive suspension were fixed and untunable during driving, the preset of k and c is important for the comfortable and vehicle handling [1]. Figure 2.7 is illustrated our scheme of optimization for passive suspension. We are in order to find the appropriate value of k and c for certain road condition. We want to get the optimization value of spring coefficient k and damping coefficient c. Therefore, we used Genetic Algorithm and according to the Genetic Algorithm and optimize of passive suspension parameters (spring coefficient k and damping coefficient c) for ATV.

If the expand and contract of ATV suspension in the normal range. Follow above, we are considering the cost functions with Genetic Algorithm. Thus, we used in the optimization was a weighted sum of the measures in equation (2-2), (2-3) and (2-3), as shown in equation (2-26) below.

$$Cost\ function = \left[\frac{RMS(a_w)}{RMS(a_{refw})}\right] + \left[\frac{RMS(\omega_{\alpha\_w})}{RMS(\omega_{\alpha\_refw})}\right] + \left[\frac{RMS(\omega_{\beta\_w})}{RMS(\omega_{\beta\_refw})}\right] \quad (2\text{-}26)$$

RMS representative is as follows

$$RMS = \left[\frac{1}{N}\sum_{n=1}^{N} a_w^2\right]^{1/2} \quad (2\text{-}27)$$

where N the number of points, a_w the frequency weighted vertical acceleration, ω_{α_w} the frequency weighted roll velocity, ω_{β_w} the frequency weighted pitch velocity.

We setting the reference RMS and compare the frequency weighted velocity and acceleration. The reference RMS are frequency weighted velocity and acceleration with not suspension install.

where a_{refw} the frequency weighted vertical reference acceleration, ω_{α_refw} the frequency weighted roll reference velocity and ω_{β_refw} the frequency weighted pitch reference velocity.

Fitness of each individual of the initial population is calculated using the cost function, equation (2-26) and is sorted in descending order. That is, the smaller value will have better fitness [1].

Chapter 3 Optimization and experiment method

3.1 Optimization method

In the chapter 2, ISO 2631-1(1997) used method (RMS) is applied in this paper and define the cost function. About the optimization algorithm, Genetic Algorithm (GA) is applied to the optimization of the suspension parameters in there [1]. GA is categorized as global search heuristics, and use techniques inspired by evolutionary biology such us inheritance, selection, crossover, and mutation [1]. Figure 3.1 shows the GA-based algorithm.

Then the selected parents and offspring construct the new population used in the next iteration of algorithm. The scheme of the procedure of GA is shown in Figure 3.2. [1] [9].

The genetic algorithm program contain following parts: initial population, cost evaluation, mate selection, crossover and mutation [1] [17]. In this paper, the programming of GA is written using MATLAB and combined with the ATV model build with simulink [1].

In this paper is using pre-obtained global optimization method of the Genetic Algorithm, calculated and simulated optimization of passive suspension parameters for ATV.

3.2 Experiment structure

The framework block diagram is shown in Figure 3.3. The block diagram illustrated this research structure. These block diagrams have two block area. However, Genetic algorithm optimization block and simulation

result have already known (blue real line). The experiment section (red dotted line) is this research thesis scope. We have optimization result of passive suspension parameters (spring coefficient *k* and damping coefficient *c*) for ATV. Due to the experiment, we get experiment data and compare before optimization result, and finding out the parameters of the ATV suspension optimize value.

Figure 3.4 are the experiment structure block diagram target and details. The experiment section (red dotted line), and the experiment section block diagrams have five items:

1. Road profile data.
2. The IMON corp. 6-axis motion platform.
3. Measurement system.
4. System identification for experiment equipment.
5. Compare & prove optimization data. – Experiment target.

About the above items, we explained in the following chapter.

3.3 Road profile data

The road profile data is collected from an ATV rally game made by IMON corp. [1]. Figure 3.5 are two kind of road profiles data from A, B, C and D. The road profile data of the game contains kinds of different road conditions. For example: off-road profile including loess, timberland, highway, sand beach and jouncing areas. When driver or player driving ATV on these areas, the setting of suspension parameters *k* and *c* will affect the feeling of the whole body vibration transferred from the road [1]. In order to improve the comfort of driver for different road conditions, we use

the road profile data as inputs $\vec{Z}_A, \vec{Z}_B, \vec{Z}_C, \vec{Z}_D$ then proceed the optimization procedure to find the optimized values of *k* and *c*[1]. In the chapter 4, we will explain for road profile data inputs.

3.4 Experiment equipment-Stewart platform

This experiment of research, we use Stewart platform to simulation and analysis ATV to travel on off-road using road profile data of the game. The Stewart platform is also known as parallel platform. The Stewart platform diagram is shown in Figure 3.6. The figure illustrated a Basic Stewart platform conformation.

The Stewart platform can be called the parallel type robot, parallel type platform or parallel type mechanism. Theoretically, as a 6 degree of freedom parallel mechanism, our used 6-axis motion platform is also classified as "Stewart motion platform"[19], and suitable for the processing of high precision or 3D curved surface. The characteristics are high precision, high rigidity and smaller. It application is extremely extensive too. For example: fly simulated training, video game or toy, milling machine/ drilling machine/ vertical & horizontal type 3 axle machine center, strength and strength distance measure, tank driver training etc.

About experiment, we cooperate with IMON corp. (Internet Motion Navigator Corp.) and use 6-axis platform- Hexglider that IMON corp. develop. Figure 3.7 is the IMON corp. 6-axis motion platform and figure 3.8 illustrated IMON corp. 6-axis motion platform / control unit / IPC. Hexglider is the first 6-axis motion base developed by IMON. It adopts a PC-based controller for use in motion control of multiple axes [19]. Online

actual testing result proves strong robustness and high reliability of Hexglider [19]. However, this platform is quite unique in linkage design and the way of movement is different than traditional hydraulic/pneumatic Stewart platform [19].

The IMON corp. 6-axis motion platform details list in table 3.1 and the main characteristics are as follows: [19]

1. The new design of universal joint allows larger kinematics angle with higher strength.
2. One-piece linkage strengthens the ratio of strength/inertia.
3. Ball screw and linear guide way enhance transmission precision.
4. Larger travel distance and angle rotation facilitate motion simulation reality of various carriers.
5. Module design of mechanism components makes assembly and maintenance more convenient.
6. Components designed and manufactured in high precision make the platform more rigid, reliable and robust.

So that, we use IMON corp. 6-axis motion platform to simulation and dynamic analysis ATV to travel on off-road using road profile data of the game. Measure passive suspension parameters of ATV and compare optimization of passive suspension parameters.

3.5 Experiment data measure-measurement system

Figure 3.4 is the experiment structure block diagram details among. In the measurement system, we measure the IMON 6-axis motion platform using gyroscope. We hope to get some measure data, the ATV to travel on

off-road using road profile data of the game. About measurement system detailed showing is as follows.

In the chapter 2, we talk about the yaw angle (γ) very small and can be neglected when driving alone a straight lane. Therefore, we want to measure roll (α), pitch (β) Angular speed, we choose the gyroscope and measure angular speed.

In addition to we talk about $\vec{Z}_0$ is the origin point of local reference in the chapter 2. Then we can derive the vertical displacement of each suspension, and for simplicity, we applied linearization by assuming α and β were small. Therefore, we want to measure Z-axis acceleration.

About experiment, we catch from the 6-axis motor encoder data and use numerical method for the forward kinematics to the IMON 6-axis motion platform movement posture. In the chapter 4, we will explain for forward kinematics.

3.6 System identification for IMON 6-axis motion platform

In chapter 2.2 and 3.4, we are derived of dynamic equations for ATV and use IMON 6-axis motion platform to simulation and analysis ATV to travel on off-road using road profile data of the game. But we must measure posture of IMON 6-axis motion platform. What's transfer function of the platform? So that, we defined the system identification procedure of IMON 6-axis motion platform have four steps:

1. Spectrum: we use the road profile data of ATV game, use Matlab FFT (Fast Fourier Transform) calculate spectrum. The road profile data

spectrum during 0~5Hz.

2. Input data: we use sweep sine signal and input to IPC. The sweep sine during 0~5Hz and 5~0Hz. Let the IMON 6-axis motion platform with sweep sine signal movements. The sweep sine and output data after forward kinematics to the IMON 6-axis motion platform movement posture is shown in Figure 3.9.
3. Output data: we get from the 6-axis motor encoder data and forward kinematics to the IMON 6-axis motion platform movements posture. In the chapter 4, we will explain for forward kinematics.
4. Estimates output: we use Matlab toolbox-system identification tool, n4sid algorithms calculation.

About the estimates output, we find out the roll, pitch and vertical axis transfer function ($H_{platform}$(s)) of the IMON 6-axis motion platform.

For vertical vibration of the IMON 6-axis motion platform, the transfer functions are $H_{platform\text{-}roll}$(s) and $H_{platform\text{-}pitch}$(s). A second order shaped curve of the form

$$H_{platform-roll}(s) = \frac{-19.36s + 2609}{s^2 + 88.67\ \mathrm{s} + 2607} \tag{3-1}$$

$$H_{platform-pitch}(s) = \frac{-17.1s + 1613}{s^2 + 64.76s + 1610} \tag{3-2}$$

has been used to approximate the weighting curve (bode diagram)and shown in Figure 3.10 and 3.11.

For rotation vibration of the IMON 6-axis motion platform, the transfer function is $H_{platform\text{-}z}$(s). A second order shaped curve of the form

$$H_{platform-z}(s) = \frac{-19.37s + 2586}{s^2 + 88.39s + 2583} \tag{3-3}$$

has been used to approximate the weighting curve (bode diagram)and shown in Figure 3.12.

Finally, optimization of passive suspension parameters, simulation and measurement results ($\ddot{z}, \dot{\alpha}, \dot{\beta}$) multiplication new frequency weighting ($H_{platform}(s) * H_{human}(s)$) and shown in Figure 3.13. We can get be closer to the frequency of the human body and experiment platform experiences in fact.

3.7 Experiment target

The experiment items and target are shown in figure 3.3 and 3.4. According to the experiment items and target diagram. First, we must installing gyroscope on the IMON corp. 6-axis motion platform. Follows above, we will input road profile data and suspension parameters of *k* and *c* to IPC. Third, measure and calculate velocity & acceleration. Fourth, compare GA optimization data. Finally, prove optimization of passive suspension parameters (spring coefficient *k* and damping coefficient *c*). Finding out the parameters of the ATV suspension optimize value.

Chapter 4 Experiment result

4.1 Initial condition define for experiment

About the initial condition for experiment have 2 items. One is the ATV model, DNM suspension and GA setting value and the other is road profile input.

We listed the ATV model physical, ATV Game default setting suspension parameters in table 4.1. We used the ATV model is ATV game setting ATV and shown in Figure 1.2. The suspension is ATV Game default setting suspension parameters. The suspensions are adjustable spring and damper design for ATV using. The default setting of suspension parameters is k=22000N/m and c=1200N-s/m [1]. The limit constraints of k is 10000<k<25000 and c is 1000<c<2500 [1]. Before optimization, we setting genetic algorithm value are listed in Table 4.2[1].

In this paper, the programming of GA is written using MATLAB and combined with the ATV model build with simulink [1]. Each individual in the population contains two parameters, spring coefficient k and damping coefficient c, which values are chosen according the constraint functions [1]. The size of initial population N_{pop} and numbers of generations are 40 and 100, and the mutate rate between 1 and 8 % often works well. In there, the number of mutate rate is 8 %.

The other is road profile input. As shown in Figure 3.5, two kinds of road profiles were used here and the left and right road profiles which pass through A, B and C, D are similar but not the same [1]. Road profile one is jouncing road with a 35 centimeters high-low variation and higher bump

frequency [1]. The number of data points is 2800, and sampling time period is 0.03 seconds. Figure 4.1 and Figure 4.2 which represent the road profiles pass through left and right of ATV, respectively. Road profile two is mild road with a 10 centimeters high-low variation and lower bumping frequency [1]. The number of data points is 2520, and sampling time period the same as road profile I. It is 0.03 seconds. As shown in Figure 4.3 and Figure 4.4. It's similarly represented left and right road profiles, respectively [1]. The road profile data input to IPC and auto control the IMON corp. 6-axis motion platform movement. Figure 4.5 illustrated the platform movement diagram and game screen.

4.2 Simulation results

In the chapter 2.2, in order to let us simulation and measurement result ($\ddot{z}, \dot{\alpha}, \dot{\beta}$) can be closer to the frequency of the human body experiences in fact. We referenced the frequency weighting curves diagram shown in Figure 2.2 [17] and get the ISO weighting curve W_k and W_e. In the chapter 3.6, optimization of passive suspension parameters, simulation and measurement results ($\ddot{z}, \dot{\alpha}, \dot{\beta}$) multiplication new frequency weighting ($H_{platform}(s) * H_{human}(s)$) and shown in Figure 3.13. We can get be closer to the frequency of the human body and experiment platform experiences in fact.

4.2.1 Road profile I-simulation result

Using the road profile I shown in Figure 4.1 and Figure 4.2 as the inputs from ground to wheels A, B and C, D [1]. Experiment result is

shown in Table 4.3. According to ATV game default setting (spring coefficient k=22000N/m and damping coefficient c=1200N-s/m), and simulation result is RMS_z=0.4533 m/s^2, J_α=1.1147 rad/s and J_β=1.3293 rad/s. Due to GA procedure, the optimized spring coefficient k=10493.5451N/m and damping coefficient c=1002.4880N-s/m. According to the optimized k and c value, and simulation result is RMS_z=0.2632 m/s^2, J_α=1.0240 rad/s and J_β=1.1394 rad/s.

Follow above, the weighted vertical acceleration $\ddot{z}$ is shown in Figure 4.6 and the zoom in figure is shown in Figure 4.7 with RMS_z attenuated from 0.4533 to 0.2632 m/s^2, the weighted roll velocity $\dot{\alpha}$ is shown in Figure 4.8 and the zoom in figure is shown in Figure 4.9 with J_α attenuated from 1.1147 to 1.0240 rad/sand the weighted pitch velocity $\dot{\beta}$ is shown in Figure 4.10 and the zoom in figure is shown in Figure 4.11 with J_β attenuated from 1.3293 to 1.1394 rad/s. We get the 16.25% improvement rate of optimized for simulation.

4.2.2 Road profile II-simulation result

Using the road profile II shown in Figure 4.3 and Figure 4.4 as the inputs from ground to wheels A, B and C, D [1]. Experiment result is shown in Table 4.4. According to ATV game default setting (spring coefficient k=22000N/m and damping coefficient c=1200N-s/m), and simulation result is RMS_z=0.4693 m/s^2, J_α=1.1130 rad/s and J_β= 1.3289 rad/s. Due to GA procedure, the optimized spring coefficient k=10198.3510

N/m and damping coefficient *c*=1015.7454 *N-s/m*. According to the optimized *k* and *c* value, and simulation result is RMS_z = 0.2816 m/s^2, J_α =0.9907 rad/s and J_β=1.1253 rad/s.

Follow above, the weighted vertical acceleration $\ddot{z}$ is shown in Figure 4.12 and the zoom in figure is shown in Figure 4.13 with RMS_z attenuated from 0.4693 to 0.2816 m/s^2, the weighted roll velocity $\dot{\alpha}$ is shown in Figure 4.14 and the zoom in figure is shown in Figure 4.15 with J_α attenuated from 1.1130 to 0.9907 rad/sand the weighted pitch velocity $\dot{\beta}$ is shown in Figure 4.16 and the zoom in figure is shown in Figure 4.17 with J_β attenuated from 1.3289 to 1.1253 rad/s. We get the 17.94% improvement rate of optimized for simulation.

4.3 Measurement result

Follow above, we listed as follow item.

1. We inputted the road profile data, suspension parameters of default setting (spring coefficient *k* and damping coefficient *c*) and optimized (spring coefficient *k* and damping coefficient *c*) value to IPC.

2. Auto control the IMON corp. 6-axis motion platform movement with the road profile I as the inputs from ground to wheels A, B and C, D. We get from the 6-axis motor encoder data and use numerical method for the forward kinematics to the IMON 6-axis motion platform movement posture.Get the IMON 6-axis motion platform movement posture (roll and pitch angle), we calculated the roll and pitch velocity. Other, we measured vertical acceleration.

About vertical acceleration measured. In the chapter 1.3 and 2.2, reduce vibration to make the passenger feel uncomfortable and the seated humans or drivers have a vertical vibration natural frequency approximate to 4~6Hz [1]. In the ATV rally game and IMON 6-axis platform, in fast, the 6-axis platform of workspace is limited, so 6-axis platform utilize washout filter. Its purpose make the platform motion keep in the workspace, reduce the 6-axis platform of movement amount and various feeling to be keep while driving at the same time.

Therefore, we get from the 6-axis motor encoder data and use numerical method for the forward kinematics to the IMON 6-axis motion platform movement posture.

4.3.1 Numerical Method for the Forward Kinematics [26]

The cockpit trajectories obtained using conventional tracking control and the proposed tracking control, are compared to demonstrate the precision of the proposed control scheme. Therefore, the six sliders must be transformed into the cockpit positions off-line; that is, forward kinematics will be used to transform the six axis coordinates into the cockpit's coordinates, including translation components and rotation components (and representing a transformation from J to S). However, direct forward kinematics is difficult to formulate for a six DOF flight simulator.

Therefore, this study proposes the use of a numerical method, such as Newton's method to execute the transformation (J to S) indirectly. The following iterative steps describe the numerical, steepest descent approach [28, 29].

1. Set k=0, and set the initial cockpit position, x_0, to the cockpit home position.
2. Calculate the present Jacobian matrix $\boldsymbol{J}_k$, according to the algorithm presented in the Appendix A.
3. Calculate the estimated errors in the positions of the six sliders as,

$$\alpha_k = p_y - p_{est,k} \in R^6 \tag{4.1}$$

where p_y is the actual positions of six slider, $p_{est,k}$ is the estimated positions of the six sliders, calculated by inverse kinematics, and α_k is the chosen step size.

4. Calculate the next estimated cockpit position,

$$x_{k+1} = x_k + \boldsymbol{J}_k \cdot \alpha_k \tag{4.2}$$

where the Jacobian $\boldsymbol{J}_k$ matrix is the equivalent gradient matrix.

5. If $\| x_{k+1} - x_k \|_2 < \varsigma$ or $\| \alpha_k \|_2 < \xi$, terminate the iteration; the approximate cockpit position is x_{k+1}, where ς and ξ are the set maximum tolerable errors.
6. Set $k = k+1$; repeat steps 2 to 5.

The convergence of this algorithm takes about two to three iterative loops, given the setting $\varsigma = 1e-12$ and $\xi = 1e-12$.

So that, the experiment structure block diagram target and details is shown in Figure 4.18.

4.3.2 Road profile I-measurement result

Experiment result is shown in Table 4.3. According to ATV game default setting (spring coefficient k=22000*N/m* and damping coefficient c=1200*N-s/m*), and experiment result is RMS_z=0.4564 m/s^2, J_α =1.0525 rad/s and J_β =1.0564 rad/s. Due to GA procedure, the optimized spring coefficient k =10493.5451 *N/m* and damping coefficient c=1002.4880 *N-s/m*. According to the optimized k and c value, and experiment result is *RMSz*=0.2665 m/s^2, J_α =0.9838 rad/s and J_β =0.9832 rad/s.

Follow above, the weighted vertical acceleration $\ddot{z}$ is shown in Figure 4.19 and the zoom in figure is shown in Figure 4.20 with RMS_z attenuated from 0.4564 to 0.2665 m/s^2, the weighted roll velocity $\dot{\alpha}$ is shown in Figure 4.21 and the zoom in figure is shown in Figure 4.22 with J_α attenuated from 1.0525 to 0.9838 rad/s and the weighted pitch velocity $\dot{\beta}$ is shown in Figure 4.23 and the zoom in figure is shown in Figure 4.24 with J_β attenuated from 1.0564 to 0.9832 rad/s. We get the 12.93% improvement rate of optimized for experiment, respectively.

4.3.3 Road profile II-measurement result

About the road profile data input, suspension parameters of default setting and optimized value to IPC and about measure step the same as the chapter 4.3 item 1 and 2.

Experiment result is shown in Table 4.4. According to ATV game default setting (spring coefficient k=22000*N/m* and damping coefficient c=1200*N-s/m*), and experiment result is RMS_z=0.4722 m/s^2, J_α =1.0498

rad/s and J_β=1.0479 rad/s. Due to GA procedure, the optimized spring coefficient *k*=10198.3510 *N/m* and damping coefficient *c*=1015.7454 *N-s/m*. According to the optimized *k* and *c* value, and experiment result is RMS_z = 0.2886 m/s^2, J_α=0.9541 rad/s and J_β= 0.9541 rad/s.

Follow above, the weighted vertical acceleration $\ddot{z}$ is shown in Figure 4.25 and the zoom in figure is shown in Figure 4.26 with RMS_z attenuated from 1.2131 to 1.0590 m/s^2, the weighted roll velocity $\dot{\alpha}$ is shown in Figure 4.27 and the zoom in figure is shown in Figure 4.28 with J_α attenuated from 0.0598 to 0.0494 rad/s and the weighted pitch velocity $\dot{\beta}$ is shown in Figure 4.29 and the zoom in figure is shown in Figure 4.30 with J_β attenuated from 0.0419 to 0.0368 rad/s. We get the 12.89% improvement rate of optimized for experiment, respectively.

4.4 Comparison

In the Table 4.3 and Table 4.4, the simulation result of road profile one and road profile two shows that the GA can efficiently converge to the optimal solution and the optimization results also show that the optimized suspension spring coefficient *k* and damping coefficient *c* can effectively attenuated vibration transmitted from road inputs [1].We compared simulation and measure results of road profile I and II.

After simulations, the simulation results have improved. The simulation result compare charts are shown in Figure 4.31~4.32. After measurement, we proved the simulation results have improved. The measure result compare charts are shown in Figure 4.33~4.34.

Road profile I weighted roll, pitch velocity and vertical acceleration compare diagrams are shown in Figure 4.35~4.40. Road profile II compare diagrams are shown in Figure 4.41~4.46. Weighted roll, pitch velocity and vertical acceleration compare measure results are similar to simulation results. The rough terrains level affects the result. In this paper, the main propose is reducing vibration to make the passenger feel uncomfortable, but the rough terrains impact the ATV body base. Therefore, we can do that the vibrations transmitted from road to human body are attenuated and the optimized *k* and *c* are found.

In this paper, the simulation results reveal that GA is suitable for the optimization design for suspension parameters of ATV and indeed reduce the RMS_z, J_α and J_β. The measure results are similar to simulation result, and the weighted vertical acceleration, weighted roll velocity and weighted pitch velocity are also improved after optimization.

Chapter 5 Conclusion

In the chapter 1.2, in order to passive suspension of ATV reduce vibration to make the passenger feel uncomfortable. A global optimization algorithm, genetic algorithm, was used in this thesis.

As to driver, the influence of roll, pitch velocity and vertical acceleration will cause driver's shaking and not comfortable feeling. We calculate the *k* and *c* value of ATV with the genetic algorithm optimization procedure, in order to improve a driver feeling not comfortable after shaking.

The main purpose of this study is the genetic algorithm optimization procedure to find out parameters of passive suspension *k* and *c*, this parameters appropriated to ATV suspension. About follow above, we used GA optimization the parameters of passive suspension *k* and *c*. We are try to process simulation, measure and verify measurement result agree with simulation result.

About the experiment, we use IMON corp. 6-axis motion platform to simulation and dynamic analysis ATV to travel on off-road using road profile data of the game. We use two kinds of road profiles with ATV rally game and to probe into optimization of passive suspension parameter *k* and *c*. The road profile data of ATV rally game input to IPC and auto control the IMON corp. 6-axis motion platform movement. We get from the 6-axis motor encoder data and use numerical method for the forward kinematics to the IMON 6-axis motion platform movement posture.

in addition the 6-axis platform utilize washout filter and prevent

platform over workspace, reduce the 6-axis platform of movement amount and various feeling to be keep while driving at the same time.

About result, these thesis finishes the works are as follows:

1. We verify pre-obtained global optimization method of the Genetic Algorithm result and used the root mean square (RMS) angular velocity are calculated and used as the assessments of discomfort of human body.
2. We cooperate with IMON corp. (Internet Motion Navigator Corp.) and use 6-axis platform- Hexglider that IMON corp. develop. We get from the 6-axis motor encoder data and use numerical method for the forward kinematics to the IMON 6-axis motion platform movement posture. Calculate roll, pitch velocity and vertical acceleration.
3. Compared the ATV game default setting and optimized weighted roll, pitch velocity and vertical acceleration. We are verifying the optimized suspension parameters k and c can reduce vibration to make the passenger feel uncomfortable.

In the feature development, first, we can be improving the suspension, carrier vibration, simulation and optimization as to the vehicle etc. Second, we hope this method can become general method for optimization design of passive suspension parameters.

Reference

[1] 徐偉鈞，「利用基因演算法設計ATV之被動式懸吊參數」，國立交通大學機械工程學系碩士論文，民96年。

[2] Gillespie, T. D. Fundamental of Vehicle Dynamics, Society of Automotive Engineering, Warrendale, PA, 1992.

[3] G.Verros, S. Natsiavas, C. Papadimitriou, "Design Optimization of Quarter-car Models with Passive and Semi-active Suspensions under Random Road Excitation", Journal of vibration and control, 11:581-606, 2005.

[4] Savaresi, S. M., Silani, E., Bittanti, S. And Porciani, N. "Decision and Control", Proceedings 42nd IEEE Conference, Vol.3, pp.2264-2269, 2003

[5] Wu, Y. and Xu, B. "Vehicle Electronics Conference", Proceeding of the IEEE International, Vol. 1, pp.66-69 Changchun, China, 1999

[6] Hashiyama, T., Furuhashi, T. and Uchikawa, Y. "Evolutionary Computation", IEEE international Conference, Vol. 1, pp.279, 1995

[7] Depez, K., Maertens, K., and Ramon, H. "American Control Conference", Proceeding of the 2002, Vol. 2, pp.1947-1501, 2002

[8] Bourmistrova, A., Storey, I., Subic, A. "Multiobjective Optimization of Active and Semi-Active Suspension Systems with Application of Evolutionary Algorithm", RMIT Business Information Systems, RMIT Mechanical and Aerospace Engineering,

[9] Niahn-Chung Shieh, Chun-Liang Lin, Yu-Chen Lin, Kuo-Zoo Liang, "Optimization design for passive suspension of a light rail vehicle using constrained multi-objective evolutionary search", Journal of Sound and

Vibration, 285, pp.407-424, 2005

[10] A.F. Naude, J.A. Snyman, “Optimization of road vehicle passive suspension systems. Part 1. Optimization algorithm and vehicle model”, Applied Mathematical Modeling, 27, pp.249-261, 2003

[11] A.F. Naude, J.A. Snyman, “Optimization of road vehicle passive suspension systems. Part 2. Qualification and case study”, Applied Mathematical Modeling, 27, pp.263-274, 2003

[12] Griffin, G.J., Rakheja, S., Sankar, S., Afework, Y. “Increased comfort and safety of drivers of off-highway vehicles using optimal seat suspension”, SAE Trans, 99, Sec 2, pp.541-548, 1990.

[13] International Organization for Standardization, ISO 2631-1. “Mechanical vibration and shock - Evaluation of Human Exposure to Whole-Body-Vibration. Part 1: General Requirements”. 1997

[14] Elbeheiry, E.M., Karmopp, D.C., Elaraby, M.E. and Abdelraaouf, A.M. “Suboptimal Control Design of Active and Passive Suspensions Based on a Full Car Model”. Vehicle System Dynamics, 26, pp.197-222, 2006

[15] Elmandany, M.M. “A procedure for Optimization of Truck Suspensions”. Vehicle System Dynamics, 16, pp.297-312, 1987

[16] Lin, J.-S and Kanellakopoulos, J. “American Control Conference”, Proceeding of the 1997, Vol. 1, pp.714-718, 1997

[17] J. C. Kirstein. “Suspension System Optimization to Reduce Whole Body Vibration Exposure on an Articulated Dump Truck”. Department of engineering, Stellenbosch University, 2005

[18]國立清華大學動力機械工程學系-精密定位系統控制實驗室網

頁 http://ppsc.pme.nthu.edu.tw

[19] IMON (Internet Motion Navigator Corp.) Web site http://www.imon.com.tw

[20] Keiichi Sawada、Masayuki Okihara、Shigeru Nakamura “A Wearable Attitude-Measurement System Using a Fiberoptic Gyroscope”, Tokimec, Inc., 2002

[21] Gyroscope introduction data, “InterTrax™ 30, InterSense Ltd”, http://www.hwp.ru/Multimedia/Glasstron/Glasstron5.html, http://www.cs.nps.navy.mil/people/faculty/capps/4473/projects/chang/intertrax.jpg

[22] Crossbow AHRS400CC ATTITUDE & HEADING REFERENCE SYSTEM specifications. http://www.xbow.com

[23] 王偉輝、許榮均、徐淵靜、洪振發，「陸上軌道運輸系統噪音振動抽測」，中華民國振動與噪音工程學會計畫編號：EPA-96-F105-02-251，2007。

[24] K. Deprez, K. Maertens, H. Ramon “Comfort improvement by passive and semi-active hydropneumatic suspension using global optimization technique”, Proceedings of the American Control Conference Anchorage, AK May 8-10, p1497-1502,2002.

[25] LEI ZUO, SAMIR A. NAYFEH, “Structured H2 Optimization of Vehicle Suspensions Based on Multi-wheel Models”,MIT USA

[26] Yang-Hung Chang, Wei-Hua Chieng, Chung-Shu Liao, Shyr-Long Jeng, “A Novel Master Switching Method for Electronic Cam Control with

Special Reference to Multi-Axis Coordinated Trajectory Following" Control Engineering Practice, No.14 p107-120, 2006.

[27] 廖俊旭,「六自由度運動模擬器之電子凸輪式追蹤運動控制策略」,國立交通大學機械工程學系博士論文，民92年。

[28] Edwin K. P. Chong and Stanislaw H. ŻAK , An Introduction to Optimization, A Wiley-Interscience Publication, John Wiley & Sons, INC., 1996, pp. 101-164.

[29] Garret N. Vanderplaats, (1984). *Numerical Optimization Techniques for Engineering Design: With Applications*. McGraw-Hill Book Company, 1984.

[30] Zhou Kemin, (1998), Essentials of Robust Control, Prentice Hall, Inc., Upper Saddle River, New Jersey, 1998, pp. 55-62, pp. 129-211

Appendix A [27]

The physical parameters of the motor may be dynamically varied, so the effect of parameter uncertainty must also be discussed. The well-known analysis of the modeling uncertainty is the μ analysis [30]. A more direct method is to analyze the sensitivities ($S_{\bar{K}}^{G_c}$, $S_{\bar{J}}^{G_c}$ and $S_{\bar{B}}^{G_c}$) of the transfer function G_c to the motor's uncertain parameters, $\bar{K}$, $\bar{J}$ and $\bar{B}$, respectively, where

$$G_c = \frac{K\bar{K}(\Im s + 1)}{K\bar{J}\Im s^2 + (K\bar{B}\Im + \bar{K}J)s + \bar{K}B} \tag{A.1}$$

$$S_{\bar{K}}^{G_c} = \frac{\partial G_c}{\partial \bar{K}} \cdot \frac{\bar{K}}{G_c} = \frac{K\bar{J}\Im s^2 + K\bar{B}\Im s}{K\bar{J}\Im s^2 + (K\bar{B}\Im + \bar{K}J)s + \bar{K}B} \tag{A.2}$$

$$S_{\bar{J}}^{G_c} = \frac{\partial G_c}{\partial \bar{K}} \cdot \frac{\bar{K}}{G_c} = \frac{-K\bar{J}\Im s^2}{K\bar{J}\Im s^2 + (K\bar{B}\Im + \bar{K}J)s + \bar{K}B} \tag{A.3}$$

$$S_{\bar{B}}^{G_c} = \frac{\partial G_c}{\partial \bar{K}} \cdot \frac{\bar{K}}{G_c} = \frac{-K\bar{B}\Im s}{K\bar{J}\Im s^2 + (K\bar{B}\Im + \bar{K}J)s + \bar{K}B} \tag{A.4}$$

Figures A.1 (a) ~ (c) show the magnitudes of the three sensitivities in relation to the input frequency, where the parameters of the master motor are all set as in Section 3.5. According to Eqs.(A.2) and (A.3), the magnitudes of the sensitivities, $S_{\bar{K}}^{G_c}$ and $S_{\bar{J}}^{G_c}$, are both small for low-frequency motion. Figures A.1 (a) and (b) reveal that the magnitudes of the sensitivities, $S_{\bar{K}}^{G_c}$ and $S_{\bar{J}}^{G_c}$, are both less than 0.707 while the input frequency is lower than $1/\Im$ (Hz). Furthermore, according to Fig.A.1(c), the magnitude of the sensitivity $S_{\bar{B}}^{G_c}$ is less than 0.00086 over the entire frequency domain. From Eqs.(A.1) ~ (A.3) and the foregoing discussion, the low time constant ($\Im$) of the disturbance estimator suppresses the

sensitivities, $S_{\overline{K}}^{G_c}$, $S_{\overline{J}}^{G_c}$ and $S_{\overline{B}}^{G_c}$.

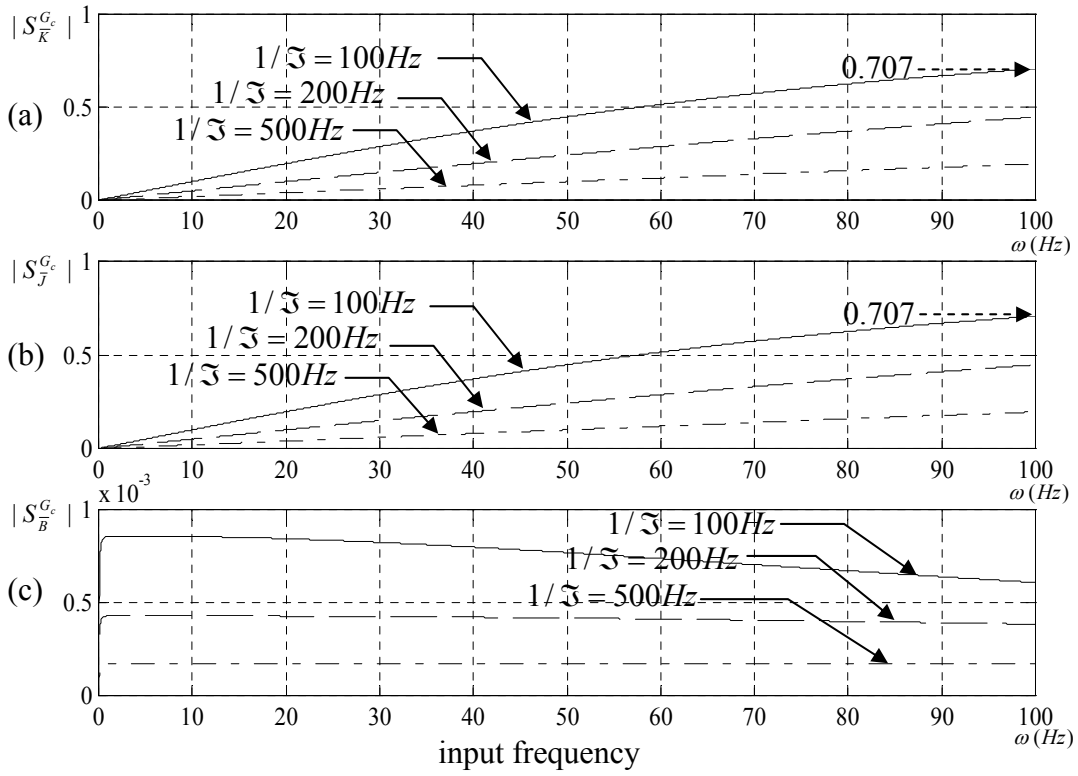

Figure A.1 Magnitudes of the sensitivities: (a) $S_{\overline{K}}^{G_c}$, (b) $S_{\overline{J}}^{G_c}$ and (c) $S_{\overline{B}}^{G_c}$,inrelation to the input frequency (ω) at various time constants ($\Im$)

Tables

Table 3.1 The IMON corp. 6-axis motion platform base details [19]

The IMON corp. 6-axis motion platform base	
Product Details	6-axis motion platform, electric-control module and IPC.
Applications	Academic – Motion control research of multi-axis simulator (such as earthquake simulation and vehicle simulation) Defense – Driver training, pilot training, shipping training Industry – Simulation platform
Main functions of the electric-control module	1. Receive IPC commands, control and drive the 6-axis motion base 2. All types of abnormal operations and power outage/braking maintenance control 3. Return to home position during machine installation 4. Collecting of absolute position data 5. System temperature control (heat exchanger, heat dissipation fan control) 6. All types of light effect controls: including base lighting and cabin lighting control 7. System power supply 8. Safety precautions during operation: prevent people from inadvertently crossing the safety line and may pose a danger during operation
IPC function	1. Real-time motion-control of motion base 2. 3D/VR texture and special-effect control 3. Real-time computing of dynamics 4. Audio control 5. Joystick control 6. Network transmission control

Table 4.1 Specification of ATV Model

ATV model	**ATV Game-ATV model physical**	
	Length	1.74 m
	Width	1.06 m
	Height	1.05 m
	Dry weight	163.44 kg
	ATV Game default setting suspension parameters	
	Spring Coefficient *k*	22000 N/m
	Damping Coefficient *c*	1200 N-s/m

Table 4.2 Genetic Algorithm setting value

	index	**value**
Genetic Algorithm	Generation number	100
	Population size	40
	Mutate rate	0.08

Table 4.3 Experiment result – Road profile I result table

Title / Items	Road profile I			
	Simulation : $H_{human}(s) * H_{platform}(s)$		Measure : $H_{human}(s) * H_{platform}(s)$	
	Before Optimized	Optimized	Before Optimized	Optimized
k(N/m)	22000	10493.5451	22000	10493.5451
c(N-s/m)	1200	1002.488	1200	1002.488
RMS_z	0.4533	0.2632	0.4564	0.2665
J_α	1.1147	1.0240	1.0525	0.9838
J_β	1.3293	1.1394	1.0564	0.9832
Cost function value	2.8973	2.4266	2.5653	2.2335
Improve rate(%)	X	16.25	X	12.93

Table 4.4 Experiment result – Road profile II result table

Title / Items	Road profile II			
	Simulation : $H_{human}(s) * H_{platform}(s)$		Measure : $H_{human}(s) * H_{platform}(s)$	
	Before Optimized	Optimized	Before Optimized	Optimized
k(N/m)	22000	10198.351	22000	10198.351
c(N-s/m)	1200	1015.7454	1200	1015.7454
RMS_z	0.4693	0.2816	0.4722	0.2886
J_α	1.1130	0.9907	1.0498	0.9460
J_β	1.3289	1.1253	1.0479	0.9541
Cost function value	2.9112	2.3976	2.5699	2.1887
Improve rate(%)	X	17.64	X	14.83

Figures

Figure 1.1 Honda TRX250EX Sport ATV.

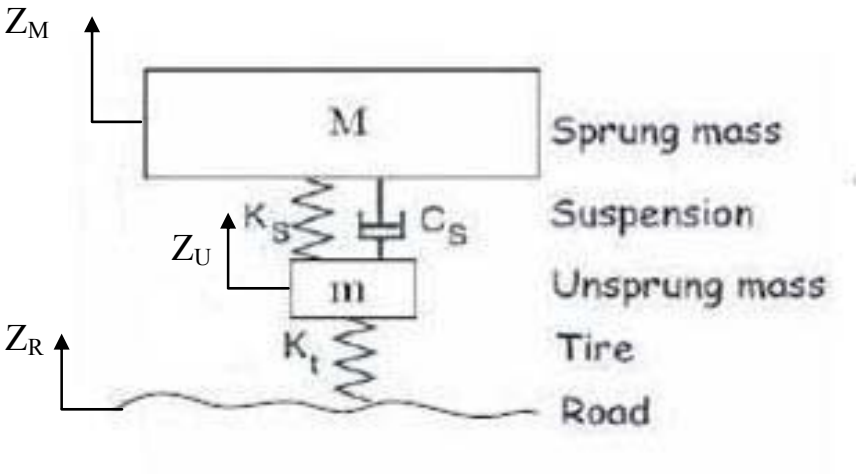

Figure 1.2 Passive suspension systems.

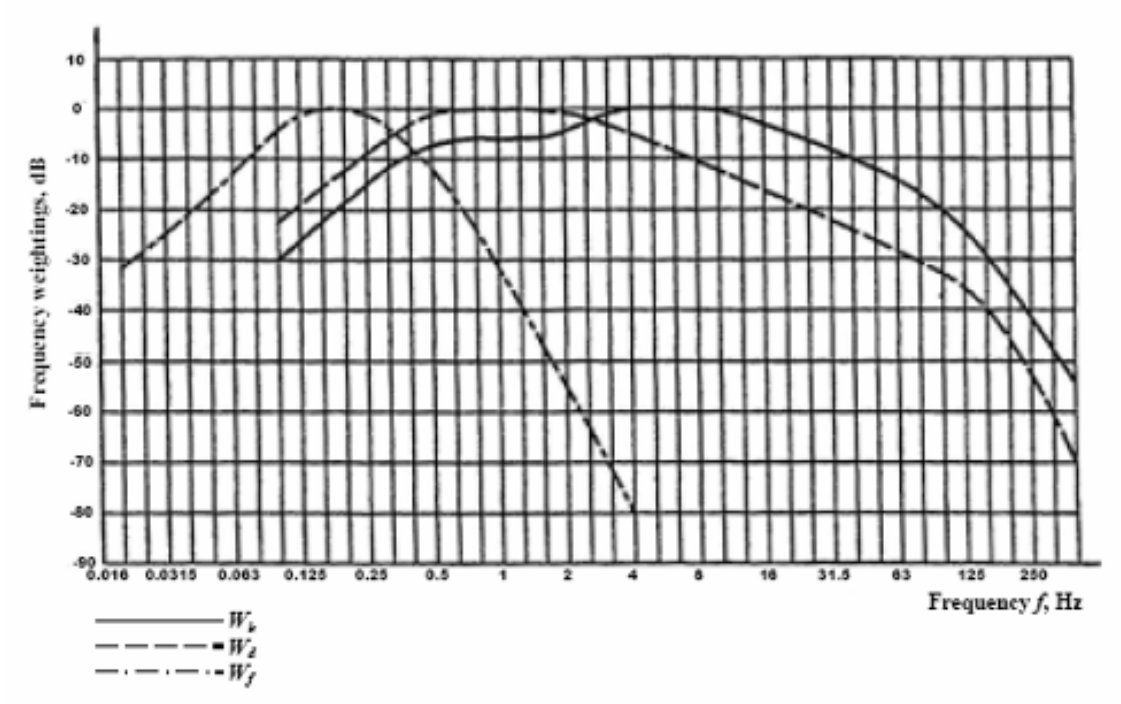

Figure 2.1 ISO2631-1:1997 Frequency weighting curves -basic [23].

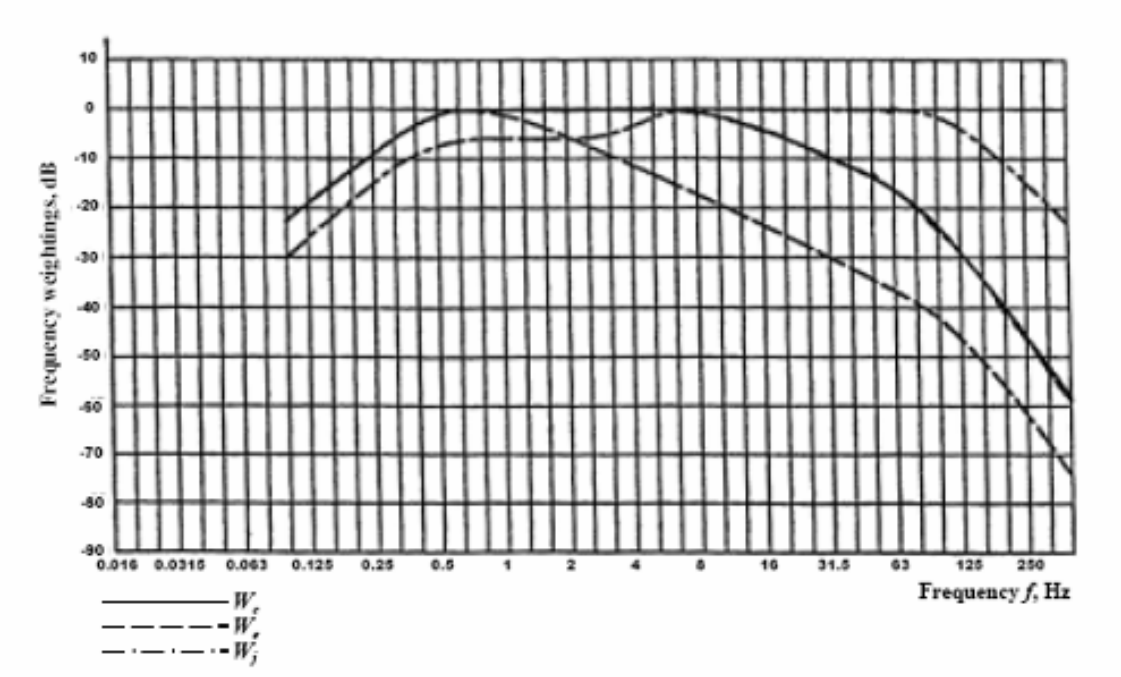

Figure 2.2 ISO2631-1:1997 Frequency weighting curves–additional [23].

Weighting filters:

z-axis : ISO 2631-1 W_k

r_x-axis : ISO 2631-1 W_e

r_y-axis : ISO 2631-1 W_e

Figure 2.3 Axes and weighting curves [13] [17].

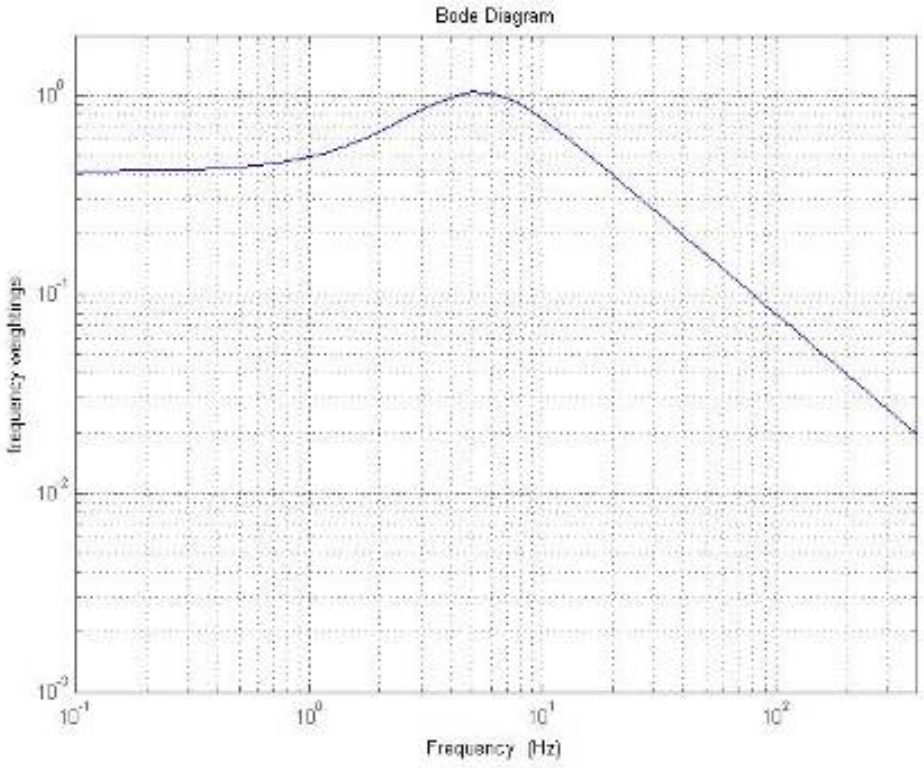

Figure 2.4 Approximate weighting curve of W_k[25].

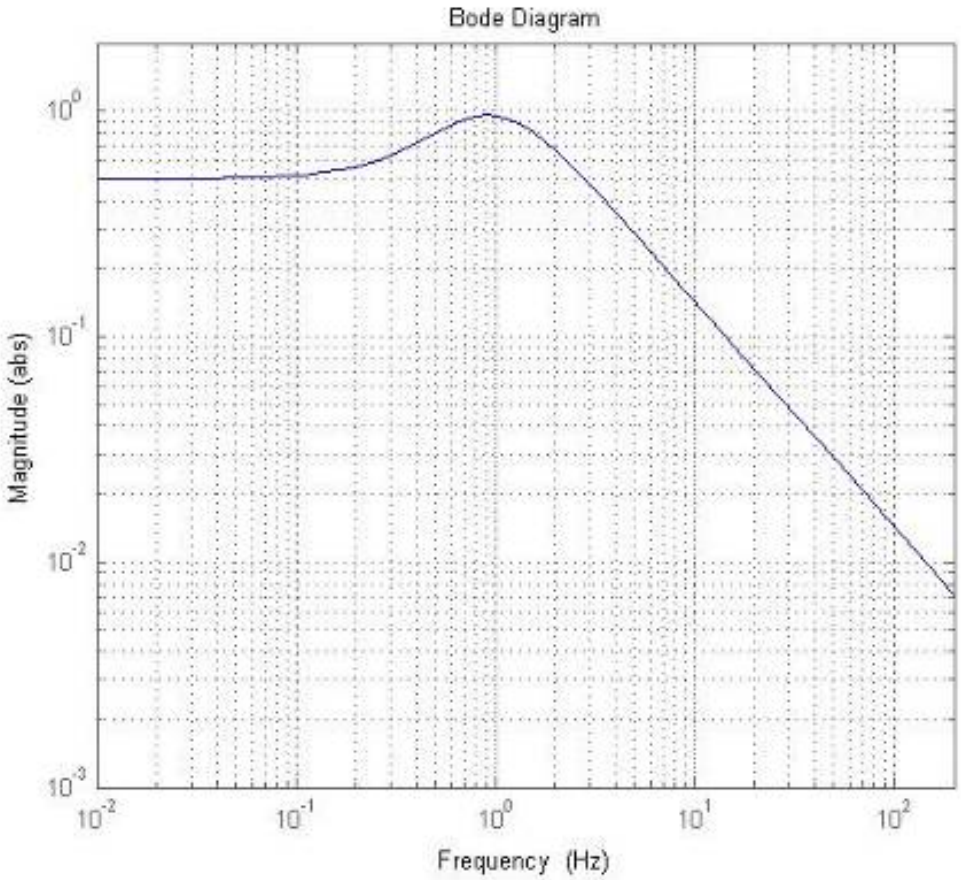

Figure 2.5 Approximate weighting curve of W_e.

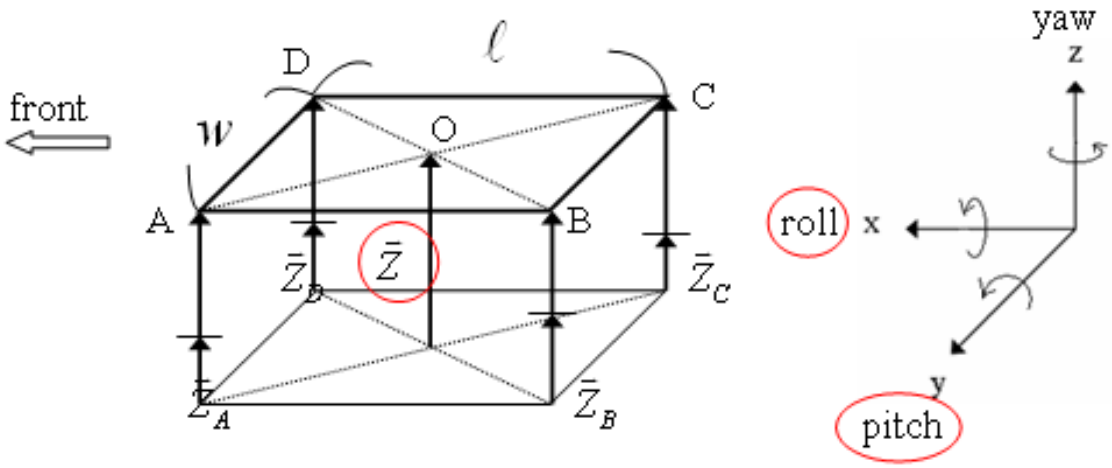

Figure 2.6 Full-car model of ATV.

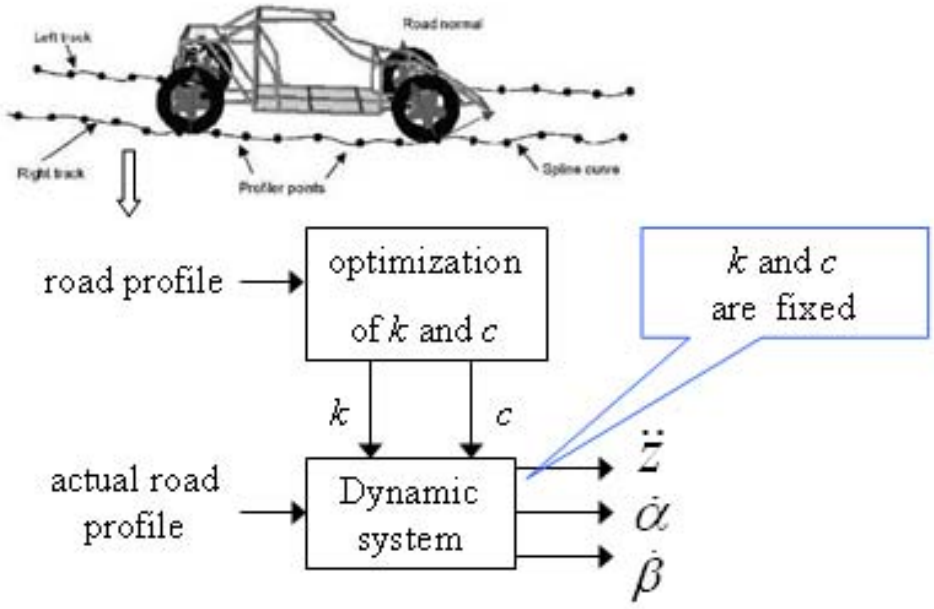

Figure 2.7 scheme of optimization for passive suspension.

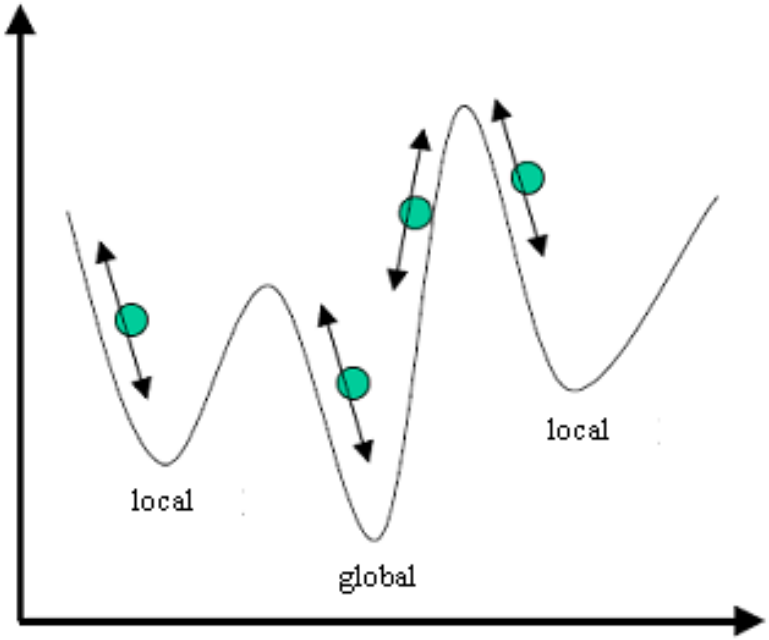

Figure 3.1 GA-based optimization algorithms.

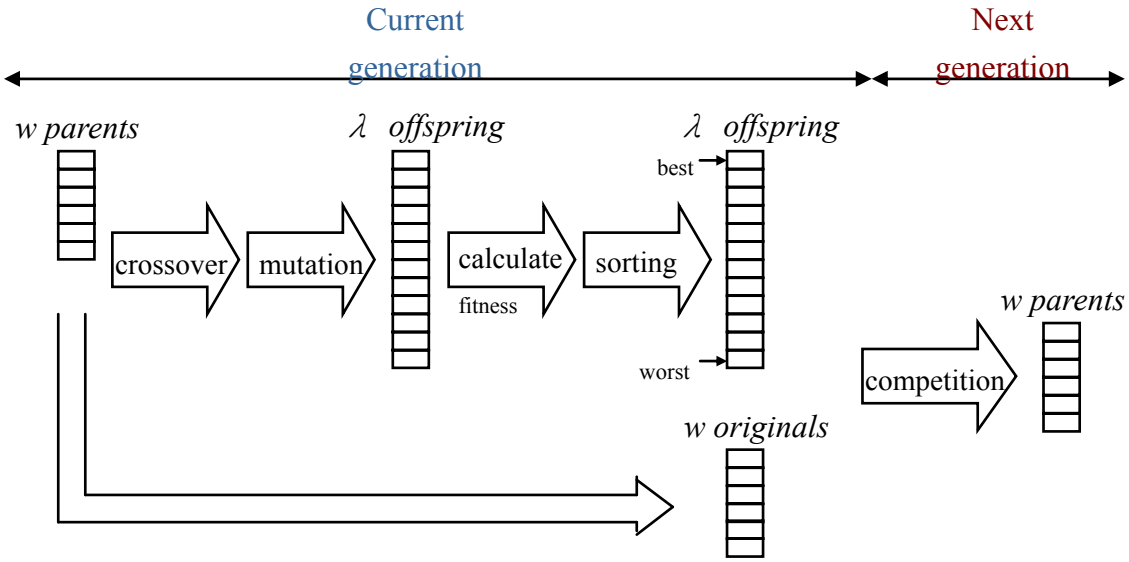

Figure 3.2 the scheme of procedure of GA (Niahn-Chung Shieh, 2005).

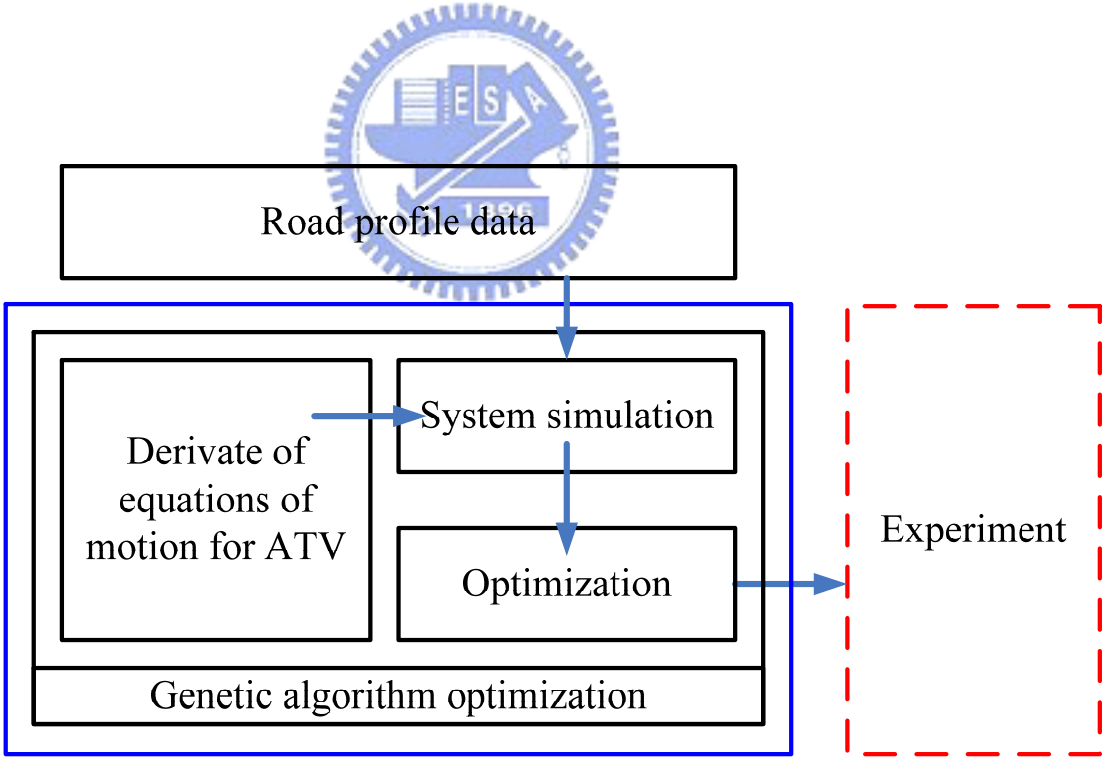

Figure 3.3 the framework structure block diagram.

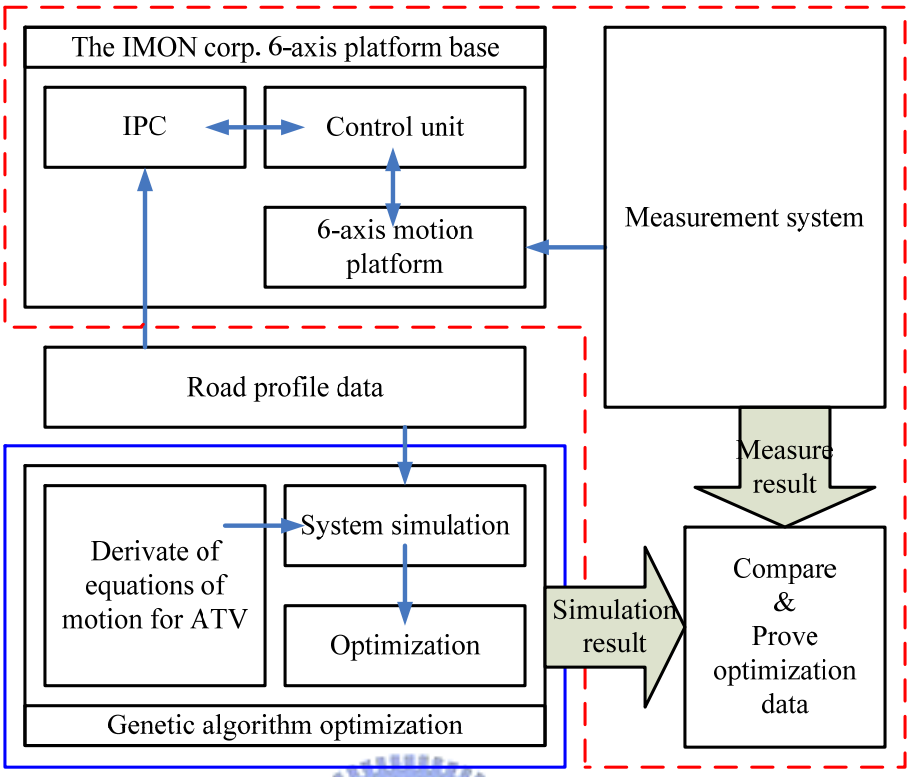

Figure 3.4 the experiment structure block diagram target and details.

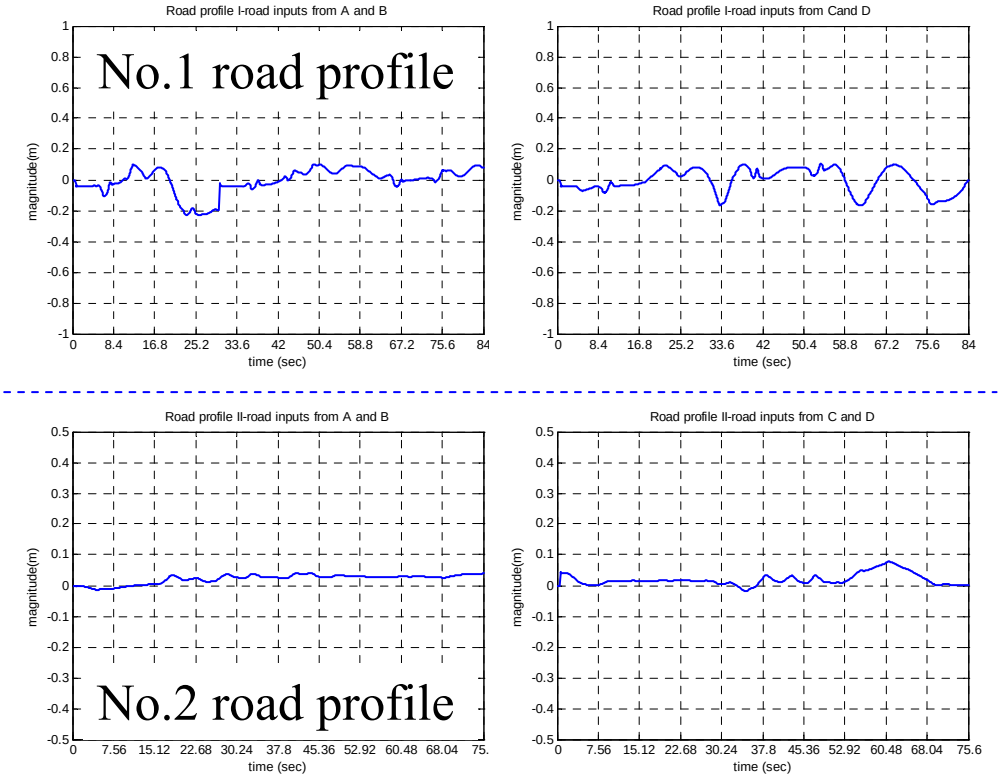

Figure 3.5 the two kind of road profile data from A, B, C and D.

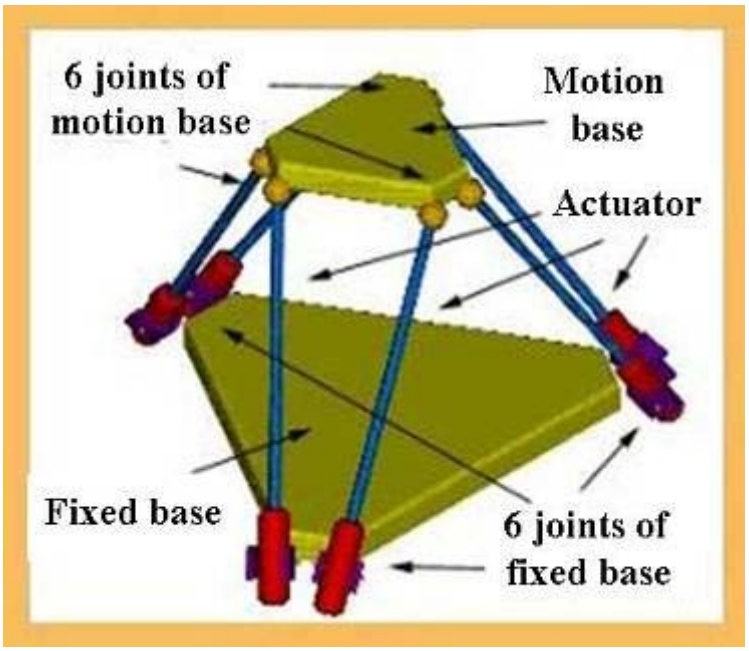

Figure 3.6 Basic Stewart platform conformations [18].

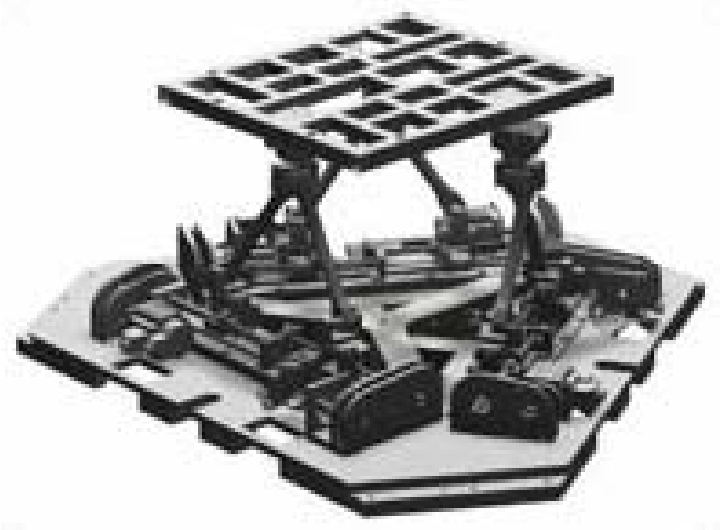

Figure 3.7 the IMON corp. 6-axis motion platform.

Figure 3.8 the IMON corp. 6-axis motion platform / control unit / IPC.

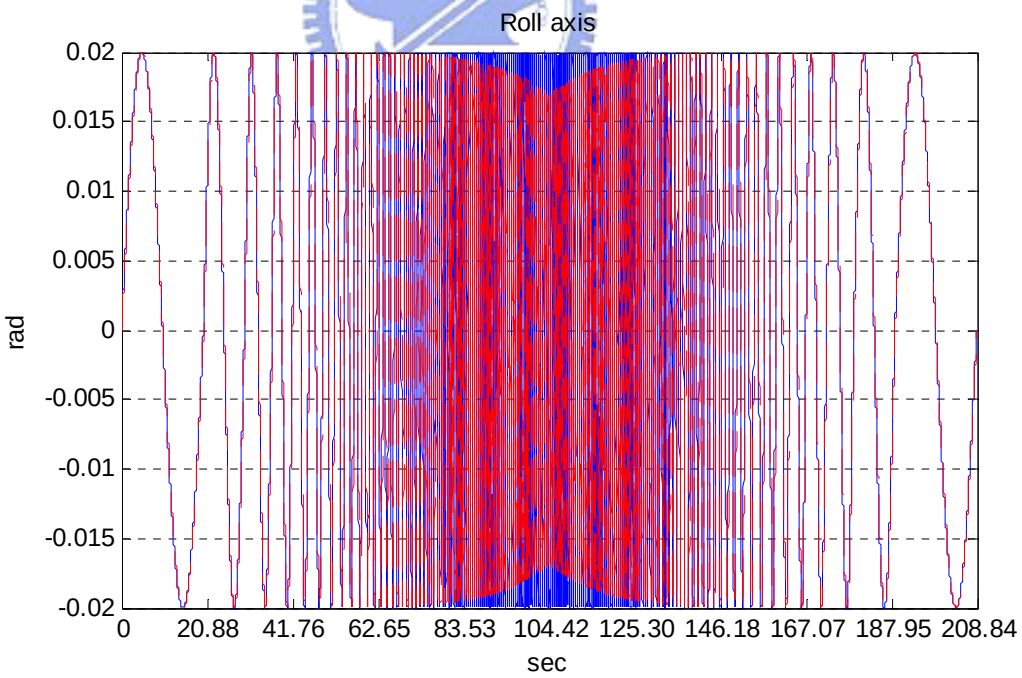

Figure 3.9 the sweep sine and after forward kinematics to platform movement posture.

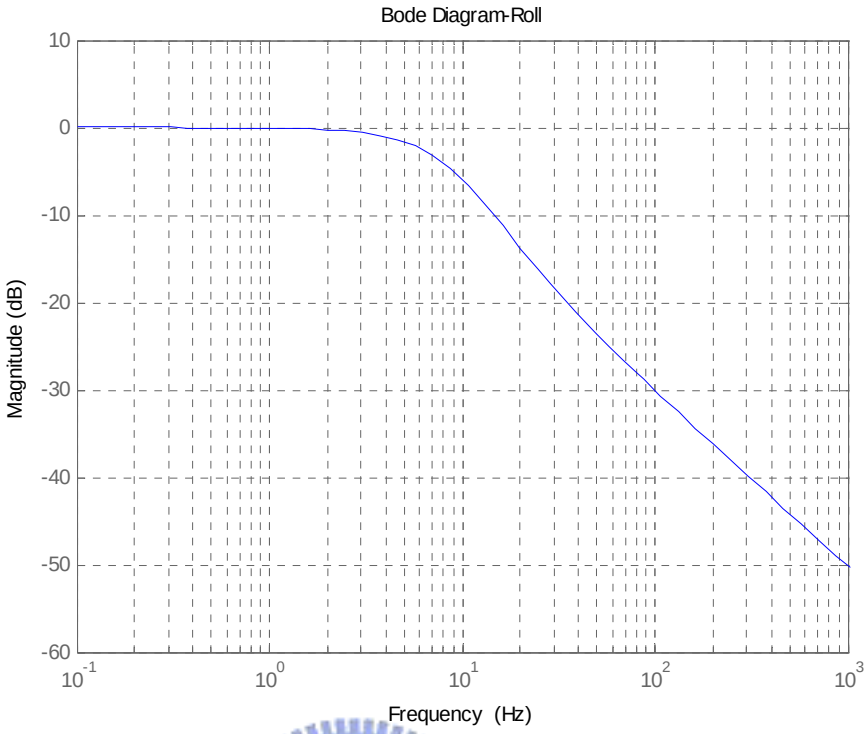

Figure 3.10 the bode diagram of transfer function $H_{platform\text{-}roll}(s)$.

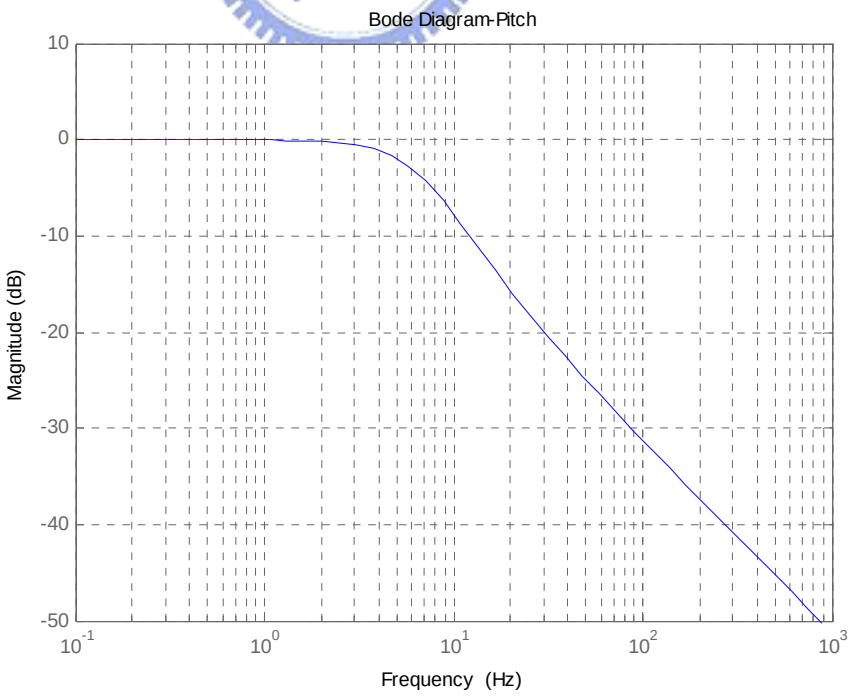

Figure 3.11 the bode diagram of transfer function $H_{platform\text{-}pitch}(s)$.

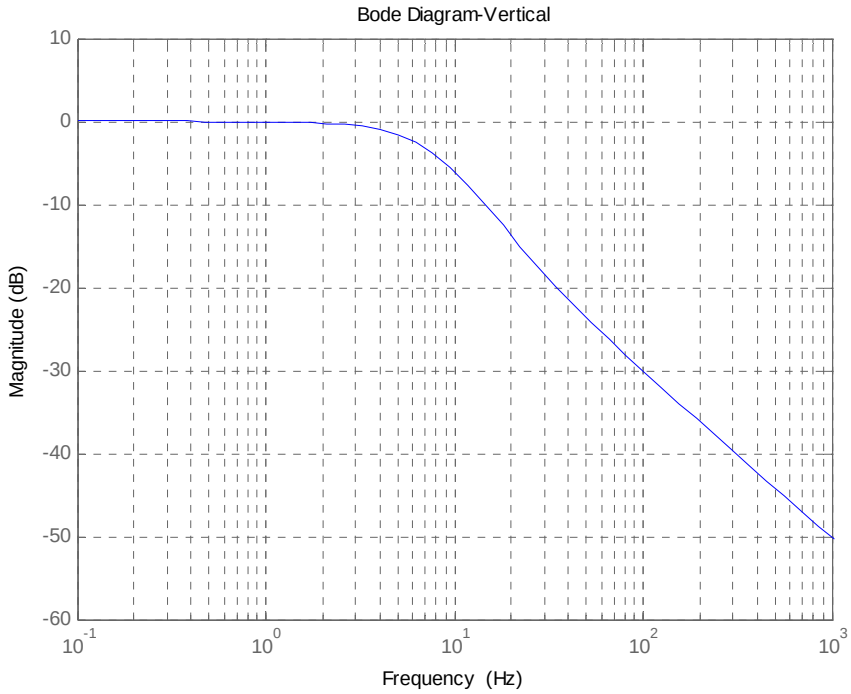

Figure 3.12 the bode diagram of transfer function $H_{platform\text{-}z}(s)$.

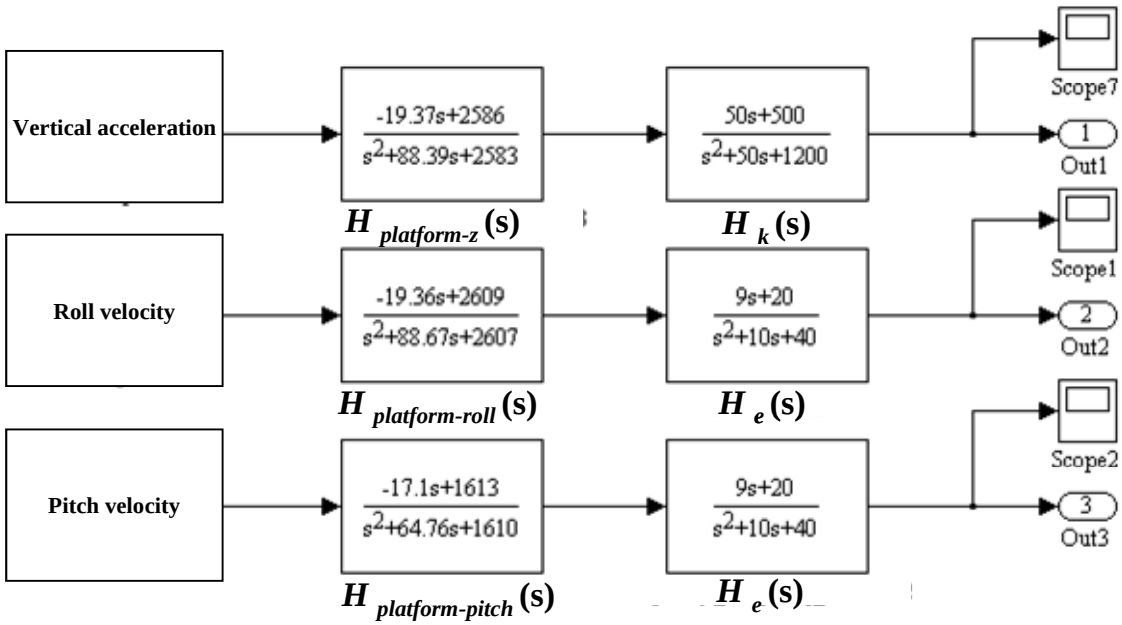

Figure 3.13 the simulink new frequency weighting $H_{platform}(s)*H_{human}(s)$.

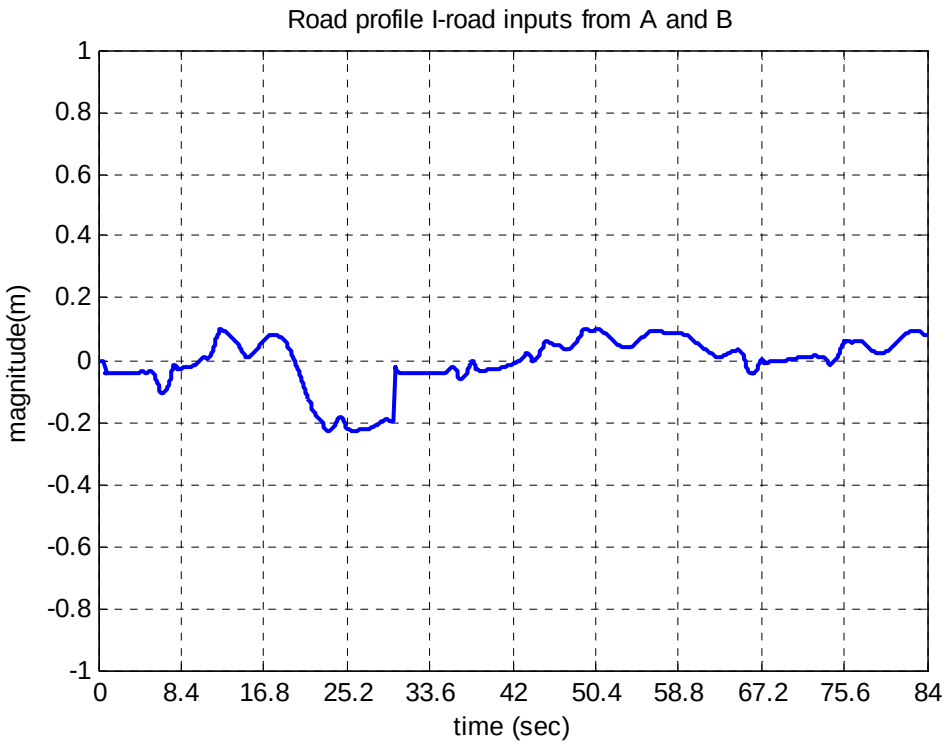

Figure 4.1 road profile I- input from A and B.

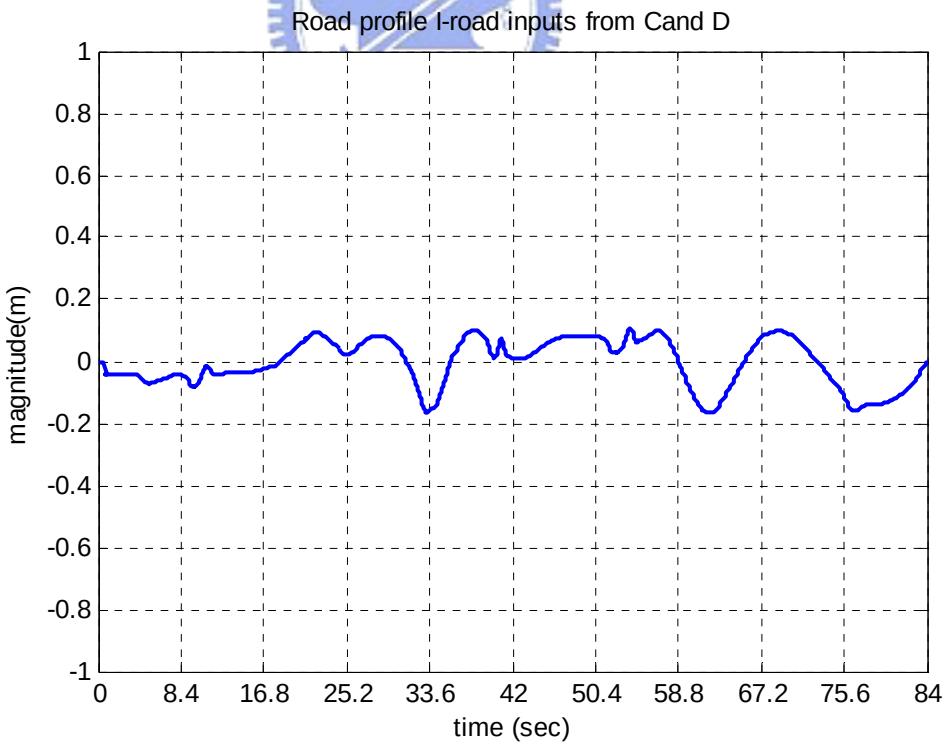

Figure 4.2 road profile I- input from C and D.

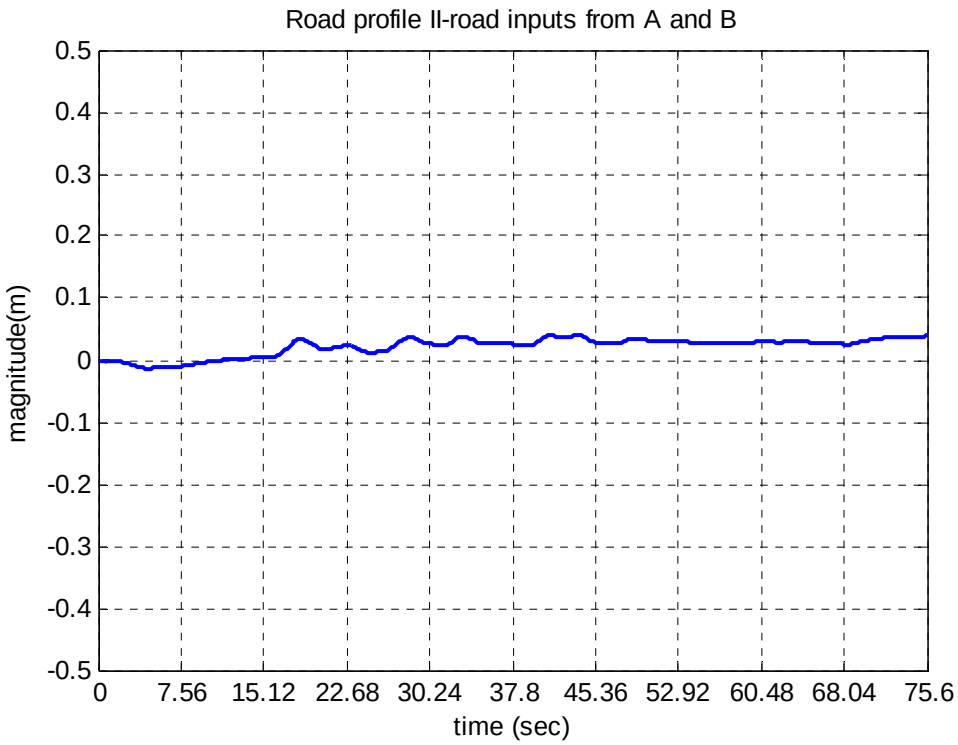

Figure 4.3 road profile II - input from A and B.

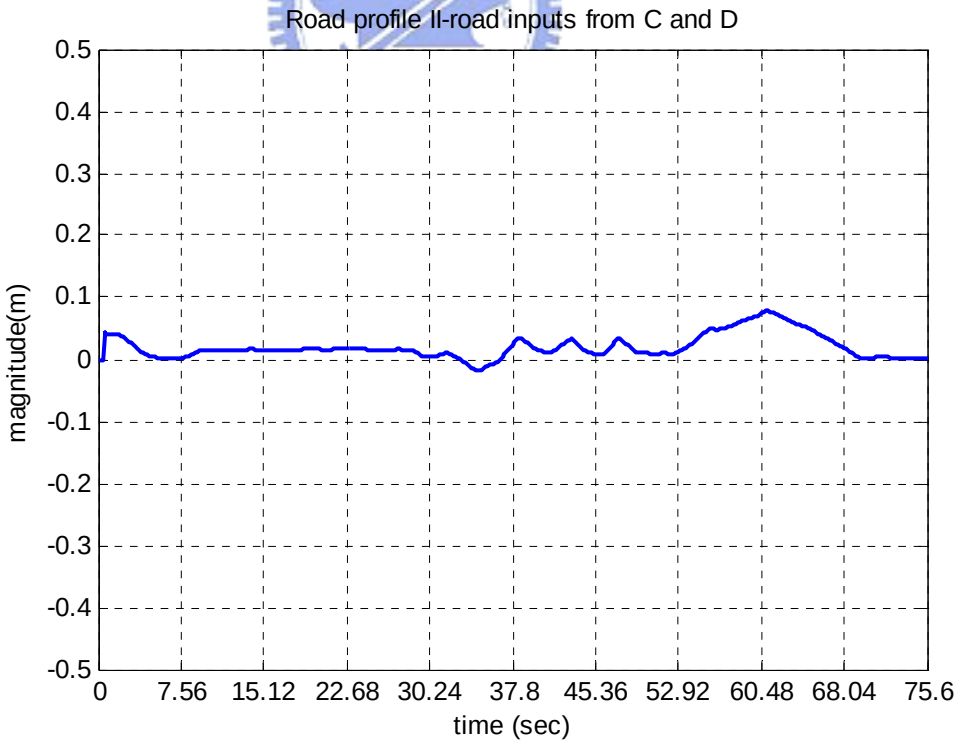

Figure 4.4 road profile II- input from C and D.

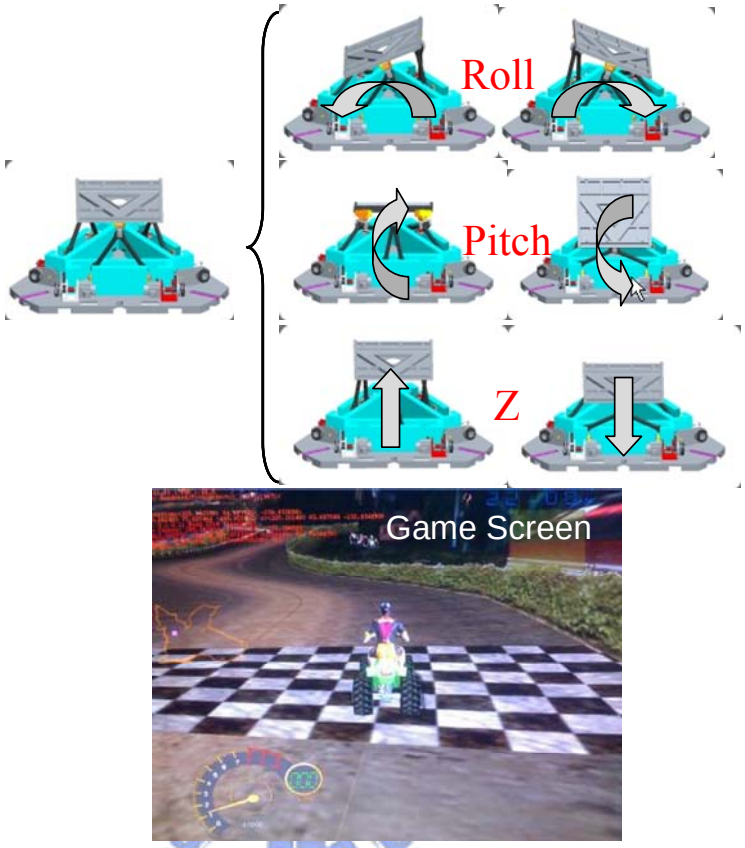

Figure 4.5 the platform movement diagram and Game screen.

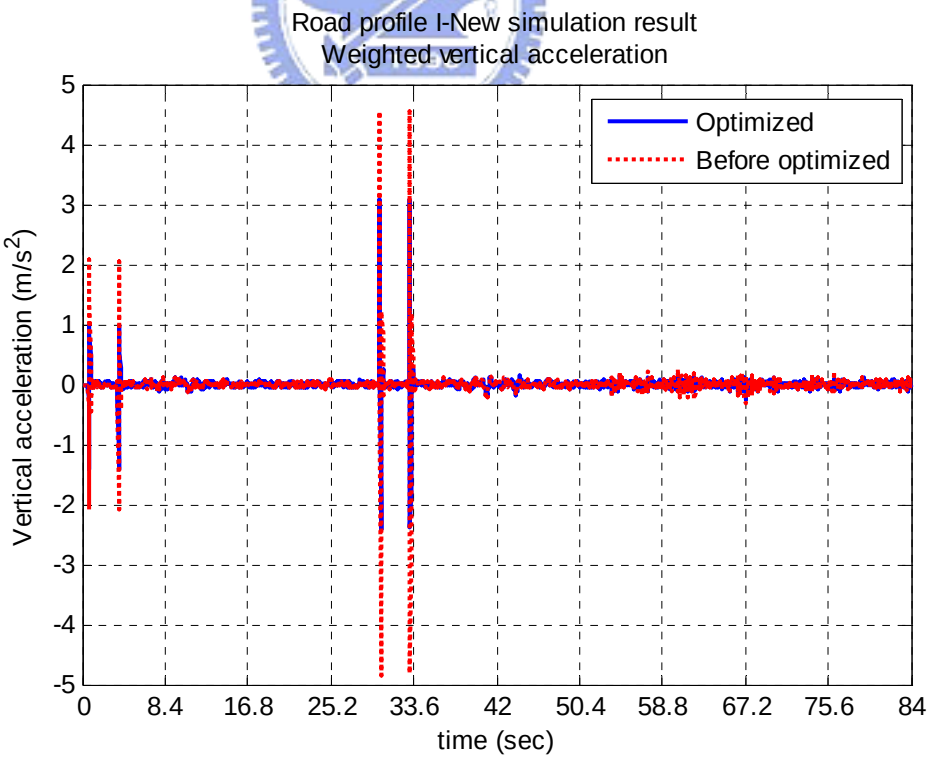

Figure 4.6 Road profile I-simulation result, weighted vertical acceleration compare.

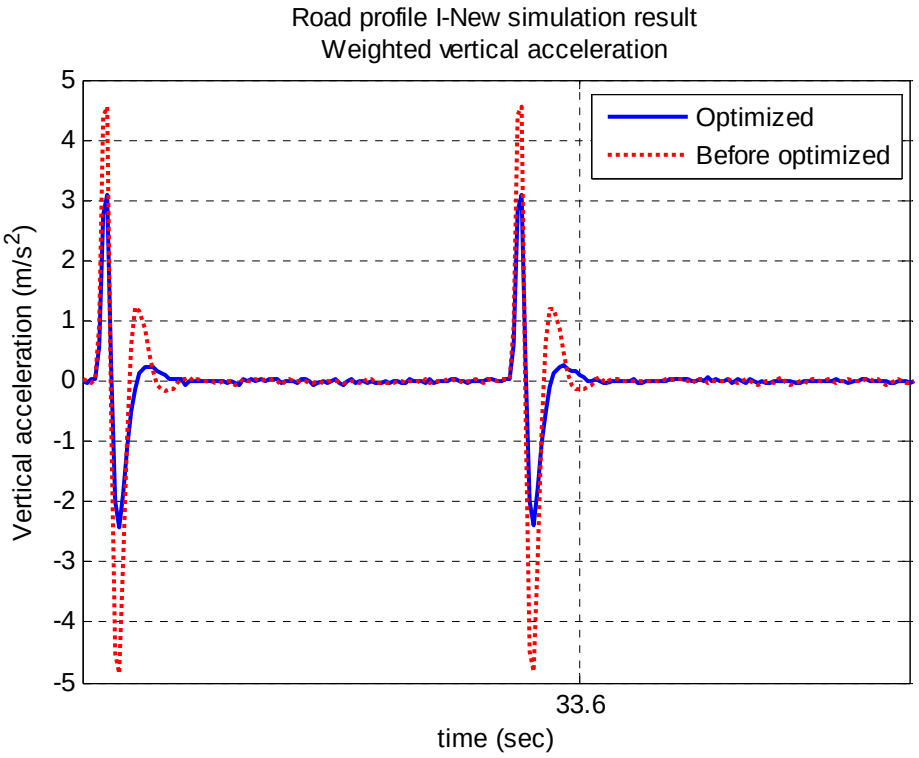

Figure 4.7 Road profile I-simulation result, weighted vertical acceleration compare between 30 and 36 sec.

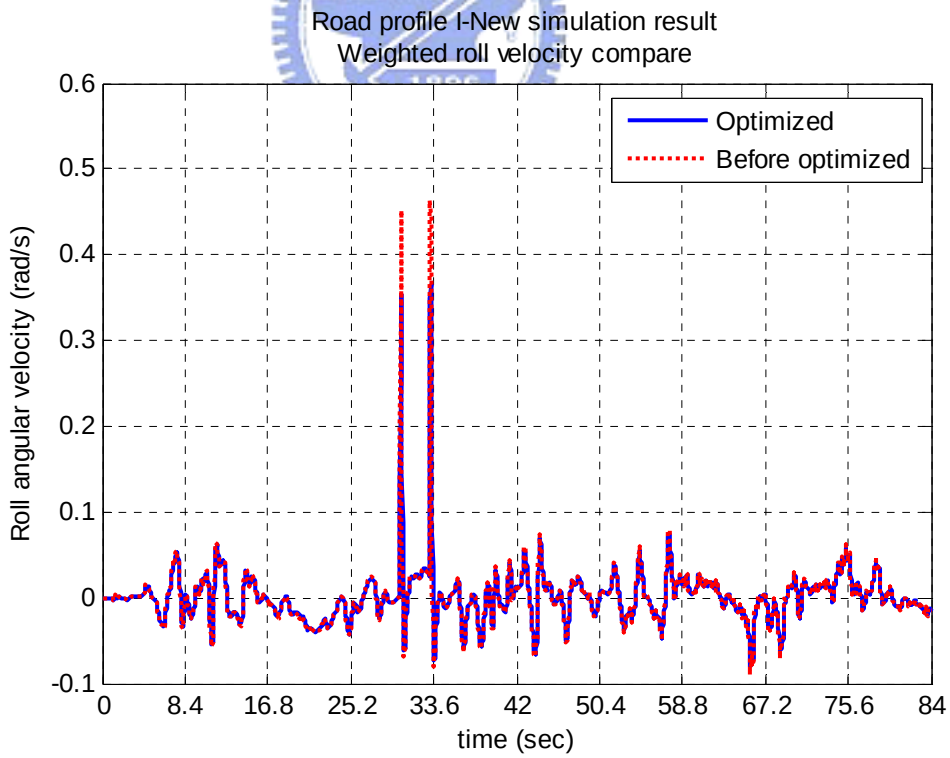

Figure 4.8 Road profile I-simulation result, weighted roll velocity compare.

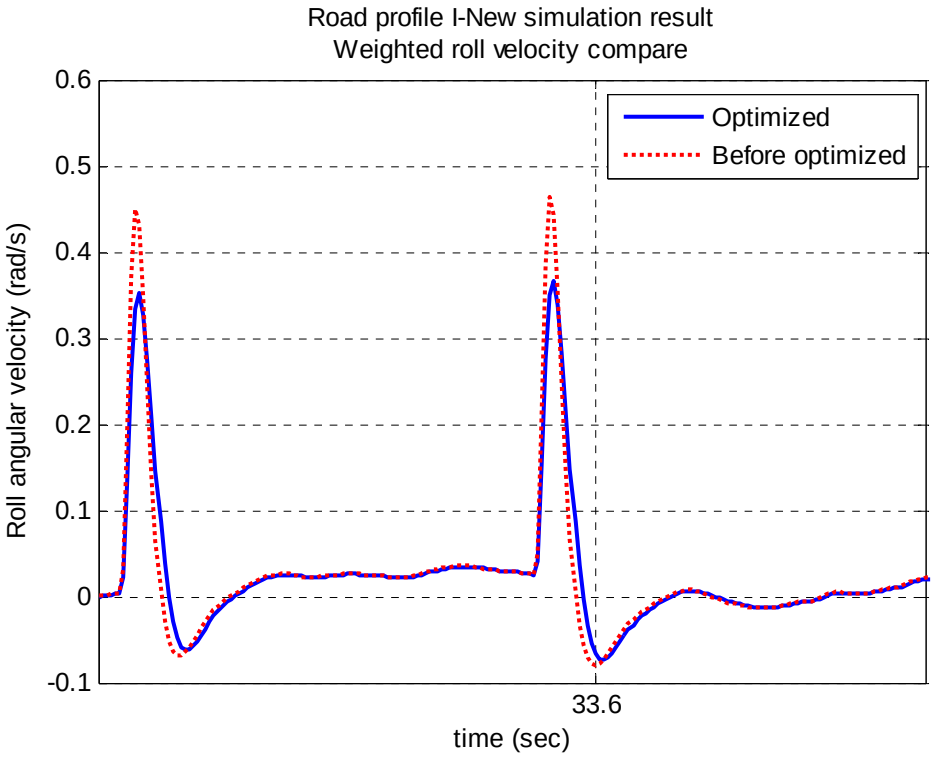

Figure 4.9 Road profile I-simulation result, weighted roll velocity compare between 30 and 36 sec.

Figure 4.10 Road profile I-simulation result, weighted pitch velocity compare.

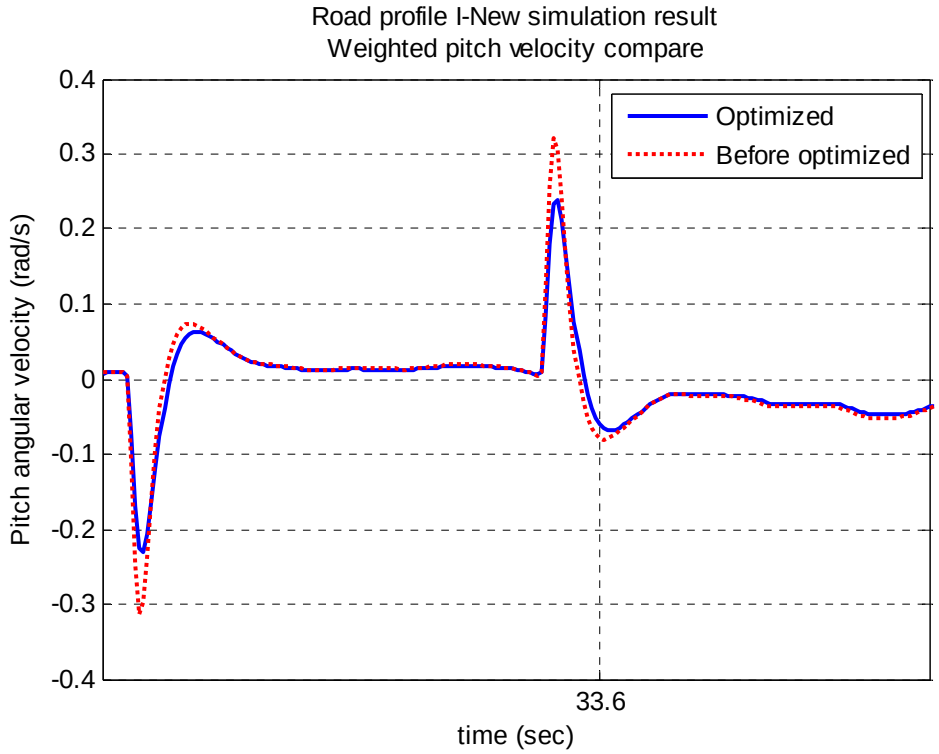

Figure 4.11 Road profile I-simulation result, weighted pitch velocity compare between 30 and 36 sec.

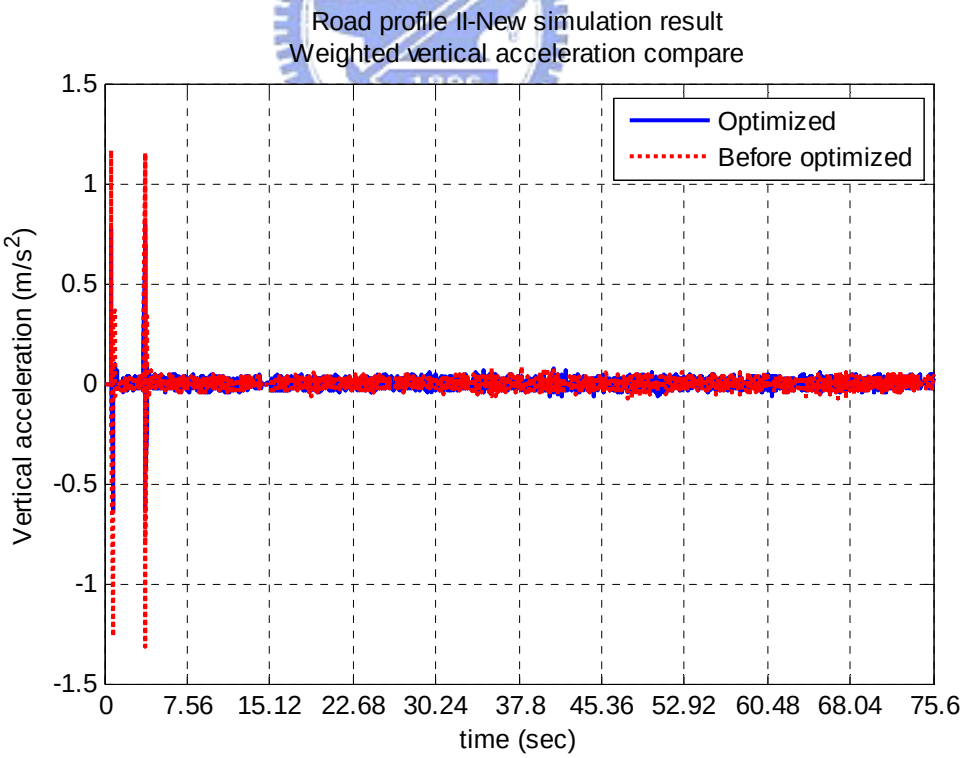

Figure 4.12 Road profile II-simulation result, weighted vertical acceleration compare.

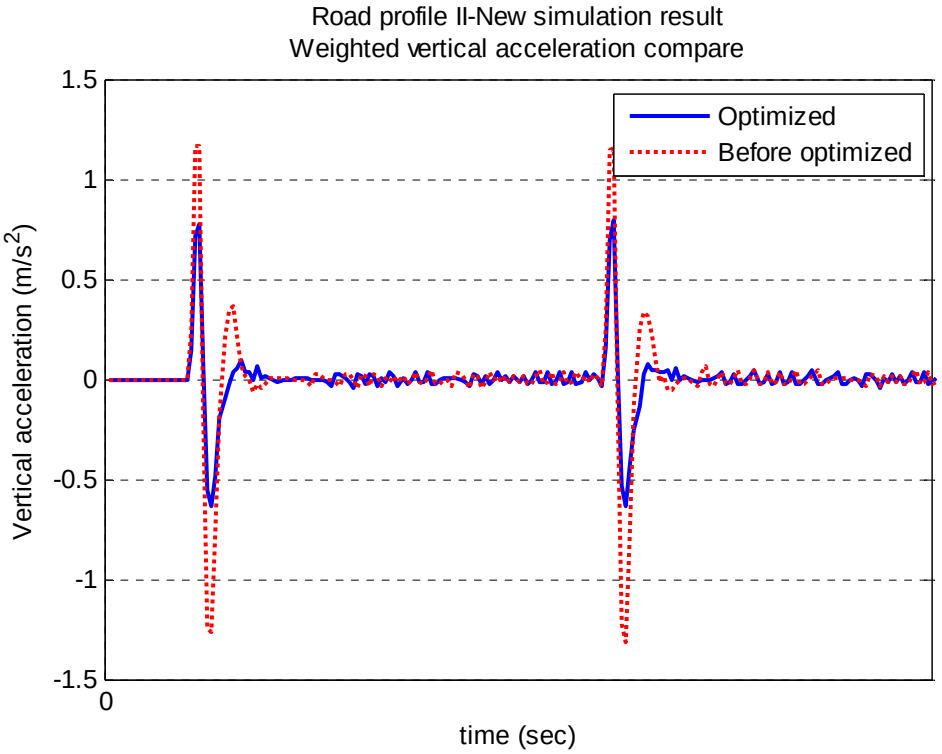

Figure 4.13 Road profile II-simulation result, weighted vertical acceleration compare between 0 and 6 sec.

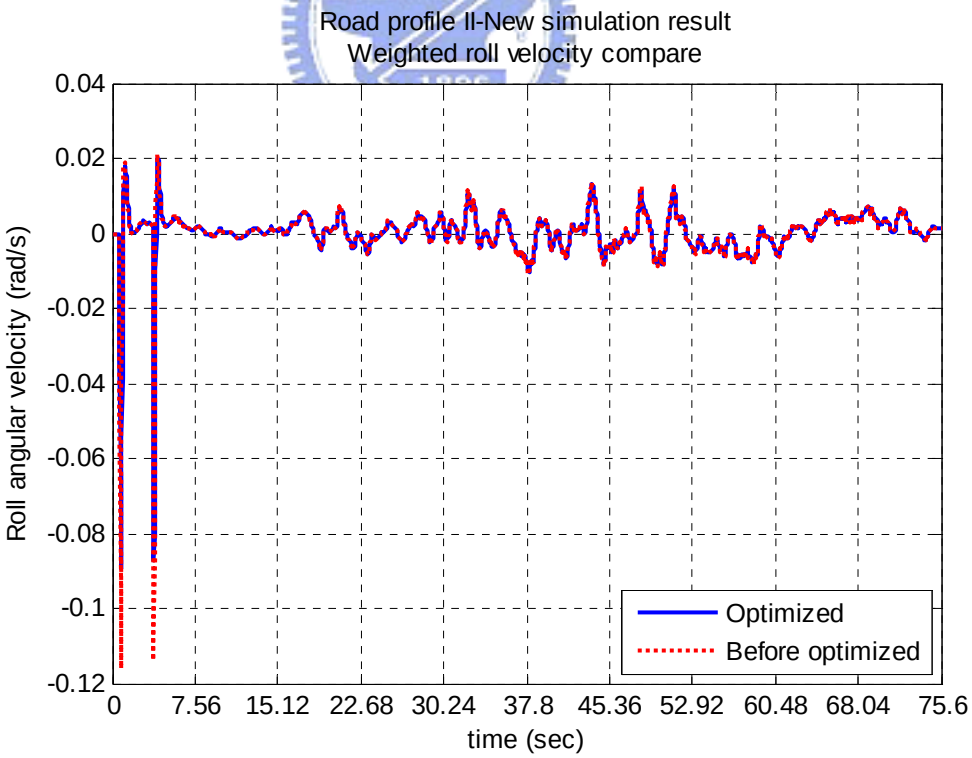

Figure 4.14 Road profile II-simulation result, weighted roll velocity compare.

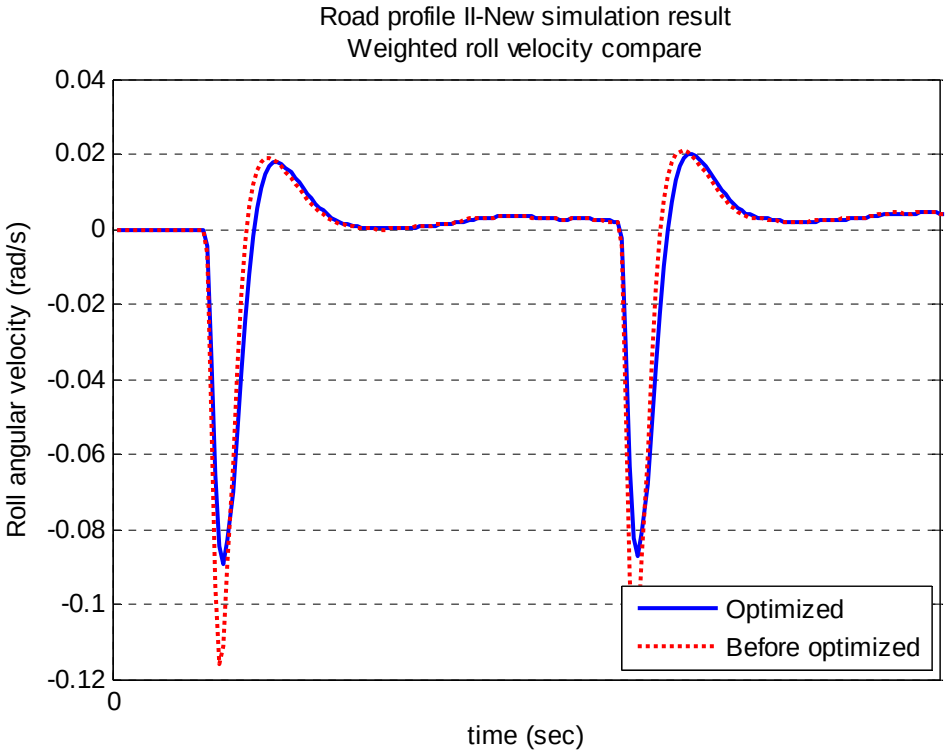

Figure 4.15 Road profile II-simulation result, weighted roll velocity compare between 0 and 6 sec.

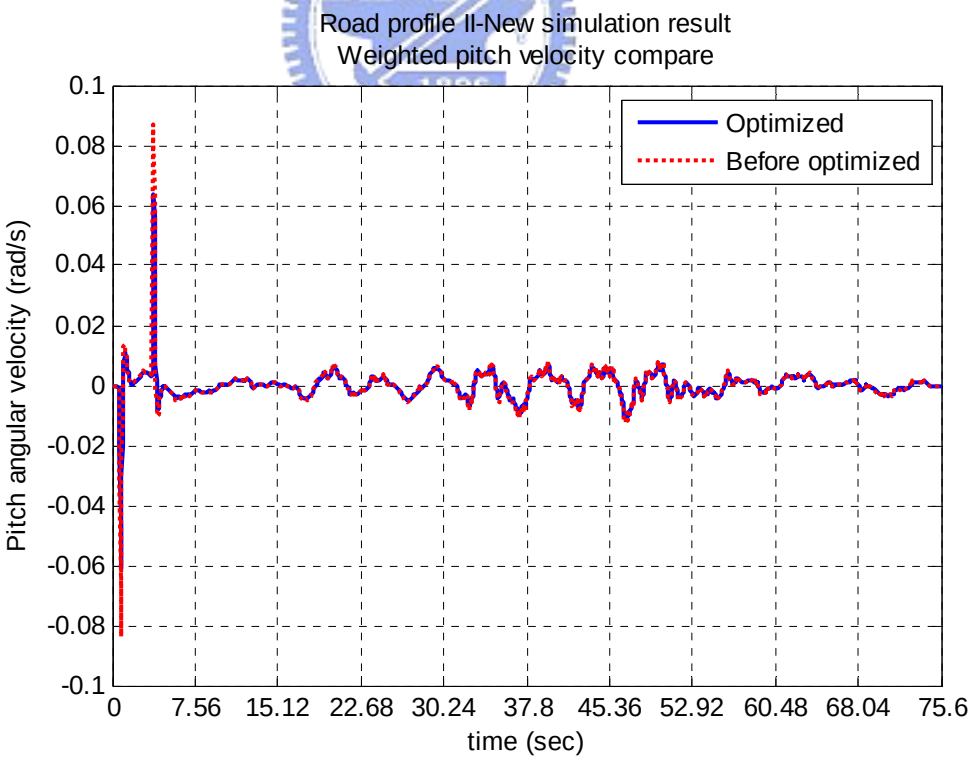

Figure 4.16 Road profile II-simulation result, weighted pitch velocity compare.

Figure 4.17 Road profile II-simulation result, weighted pitch velocity compare between 0 and 6 sec.

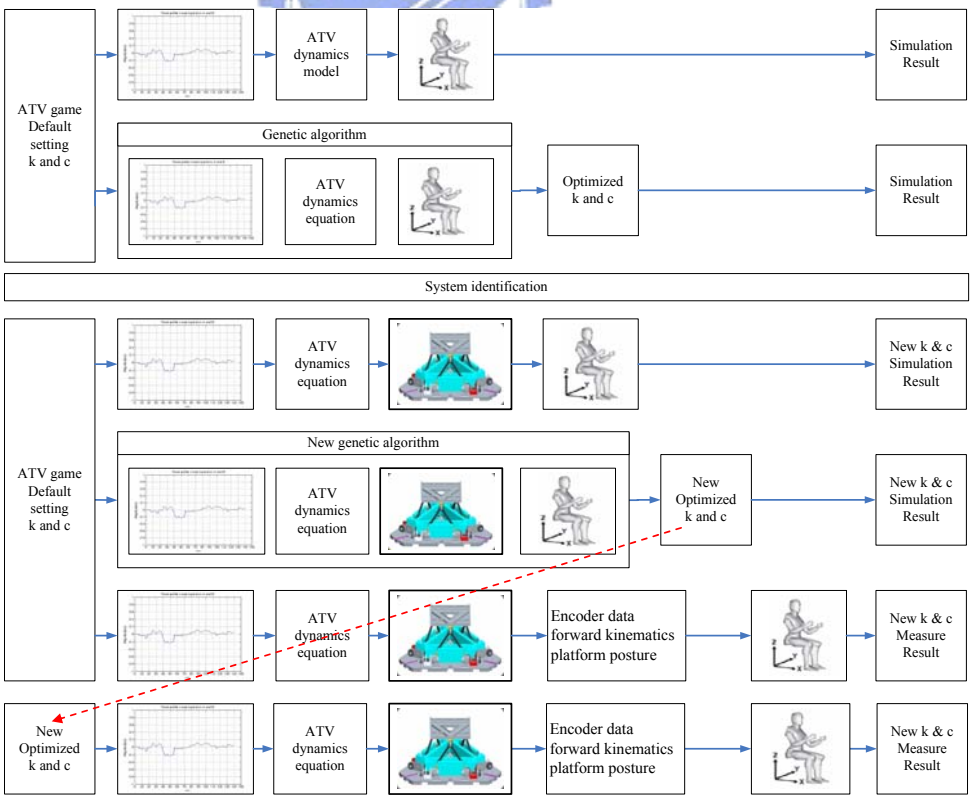

Figure 4.18 the experiment structure block diagram target and details.

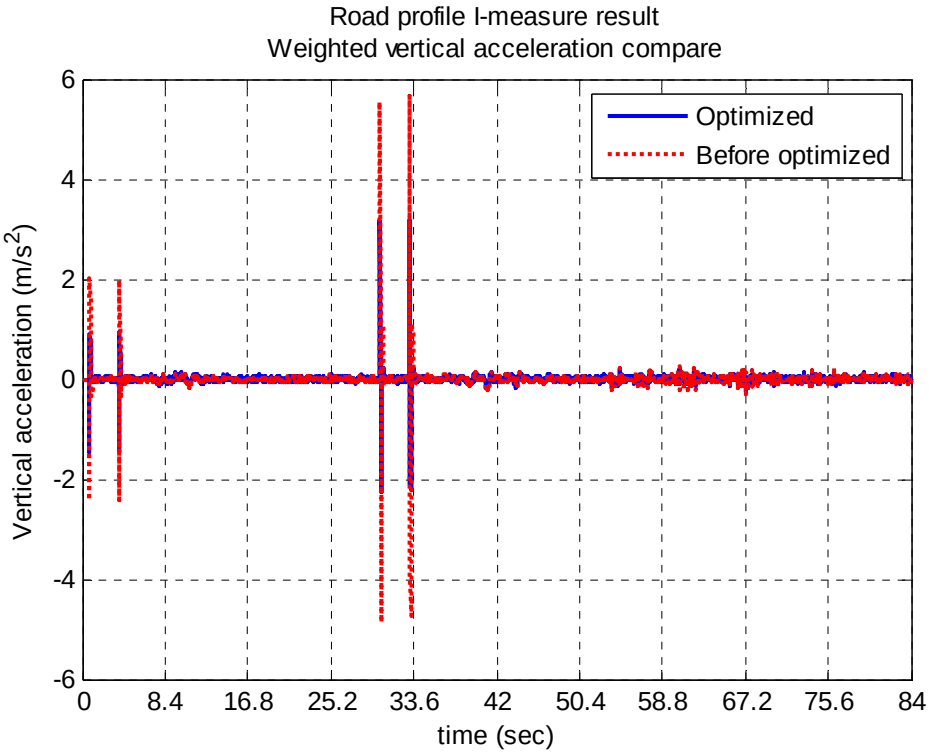

Figure 4.19 Road profile I-measure result, weighted vertical acceleration compare.

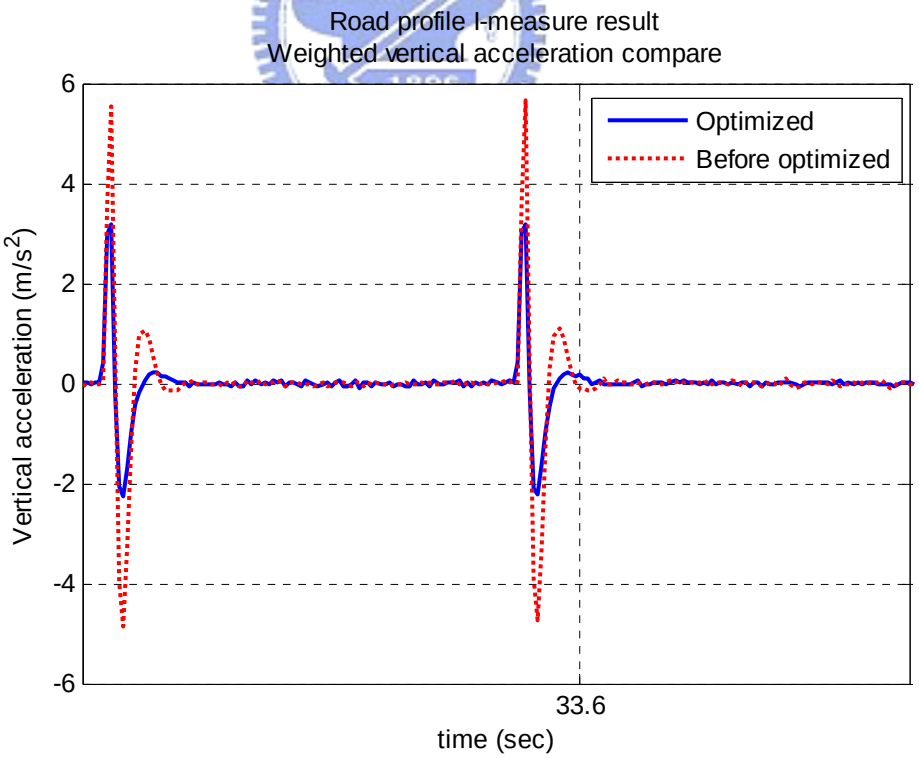

Figure 4.20 Road profile I-measure result, weighted vertical acceleration compare between 30 and 36 sec.

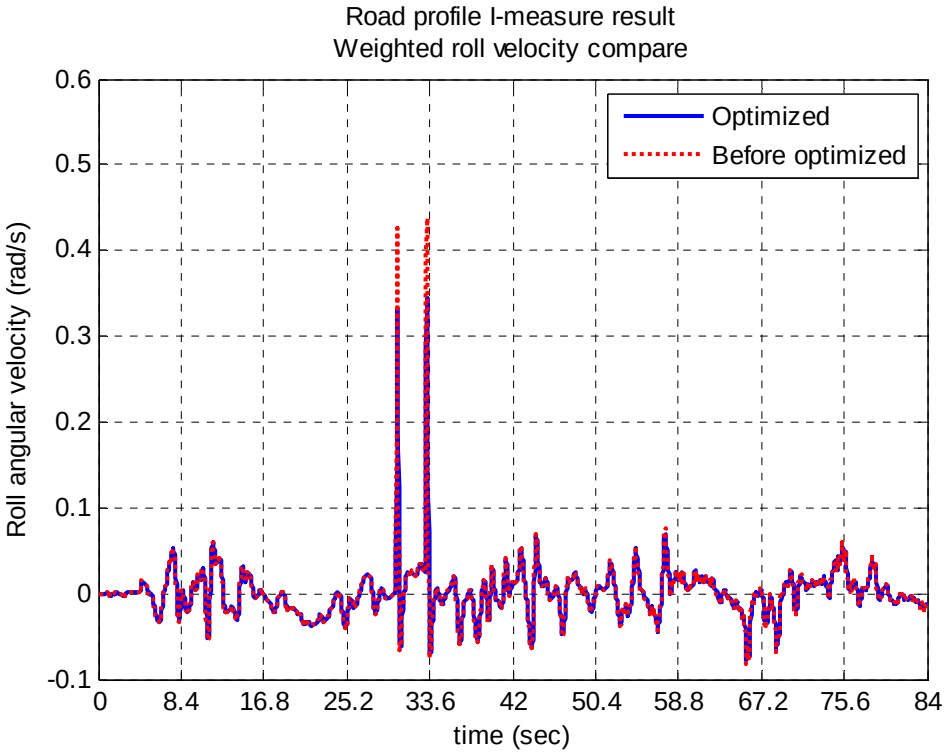

Figure 4.21 Road profile I-measure result, weighted roll velocity compare.

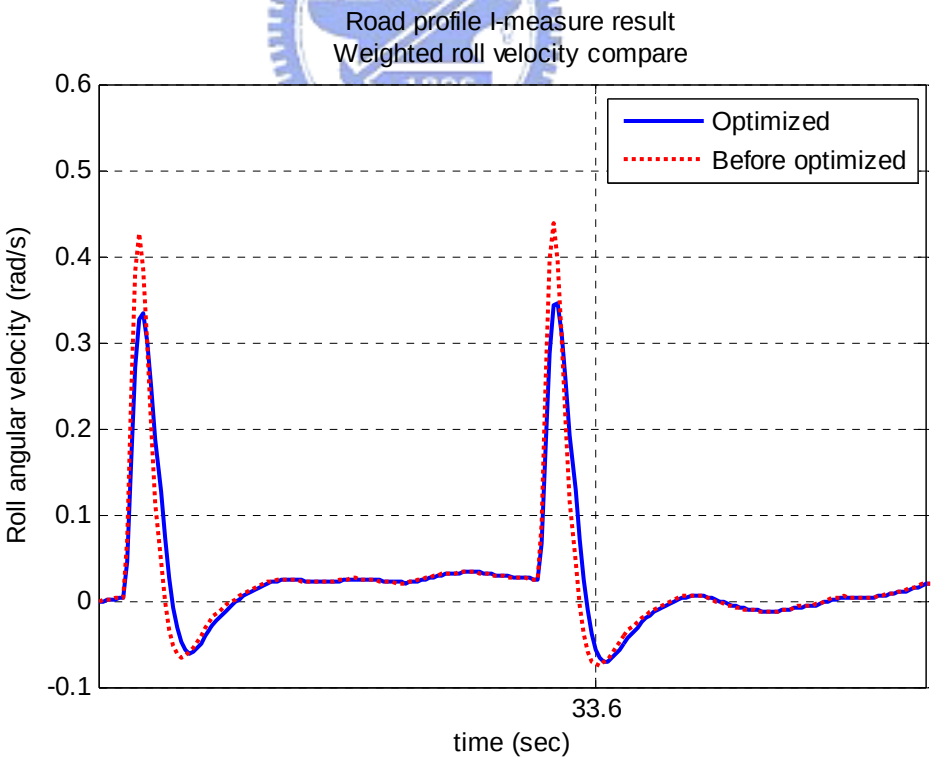

Figure 4.22 Road profile I-measure result, weighted roll velocity compare between 30 and 36 sec.

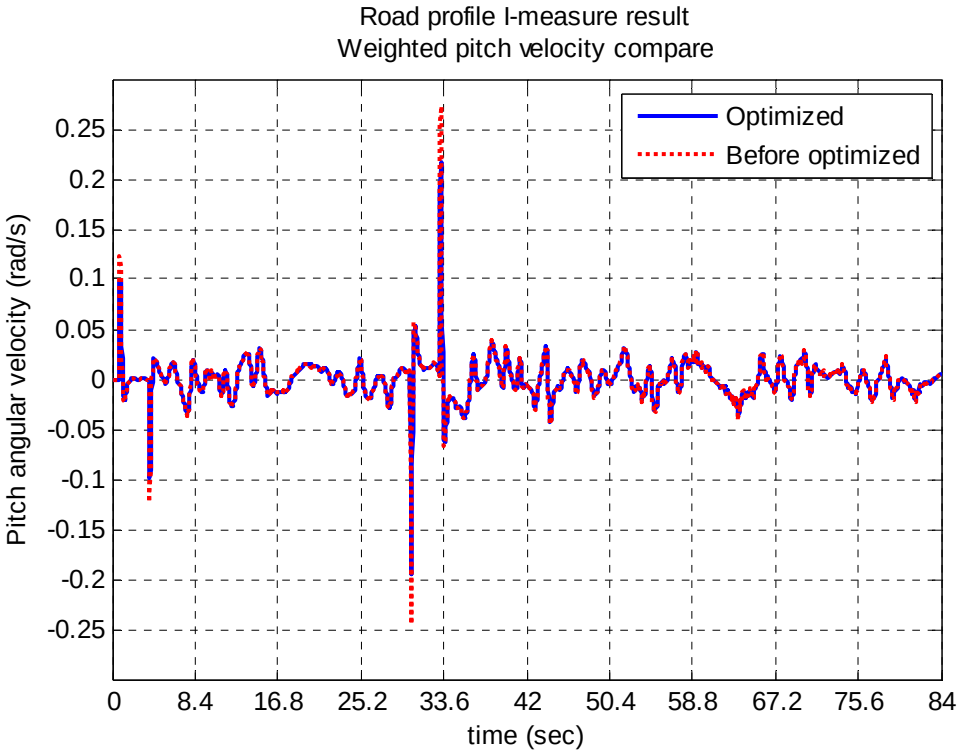

Figure 4.23 Road profile I-measure result, weighted pitch velocity compare.

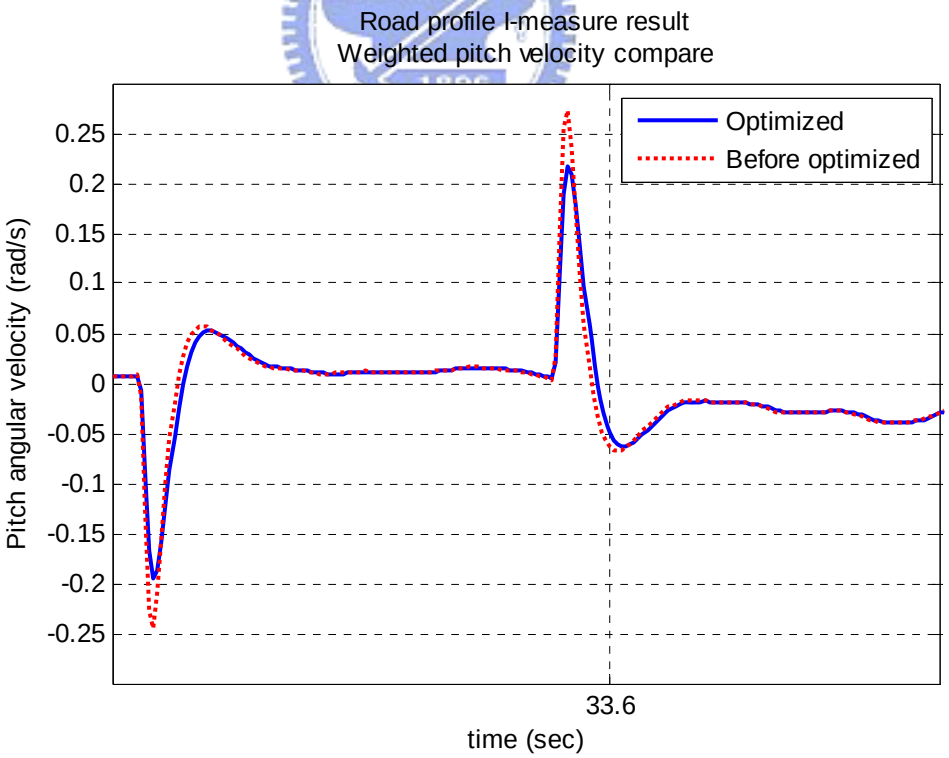

Figure 4.24 Road profile I-measure result, weighted pitch velocity compare between 30 and 36 sec.

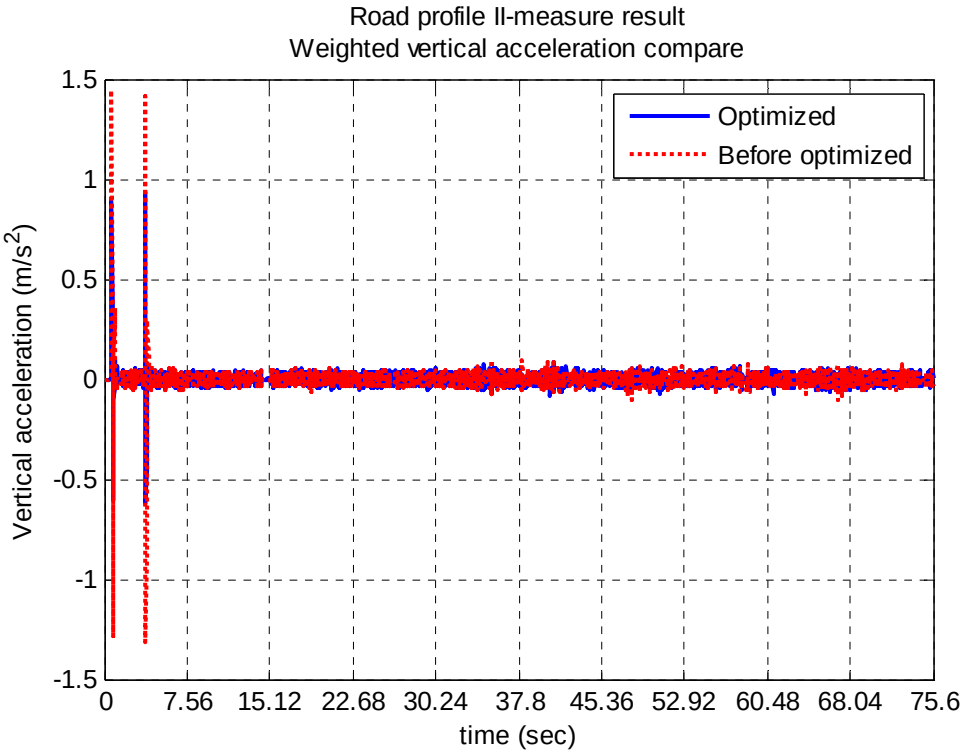

Figure 4.25 Road profile II-measure result, weighted vertical acceleration compare.

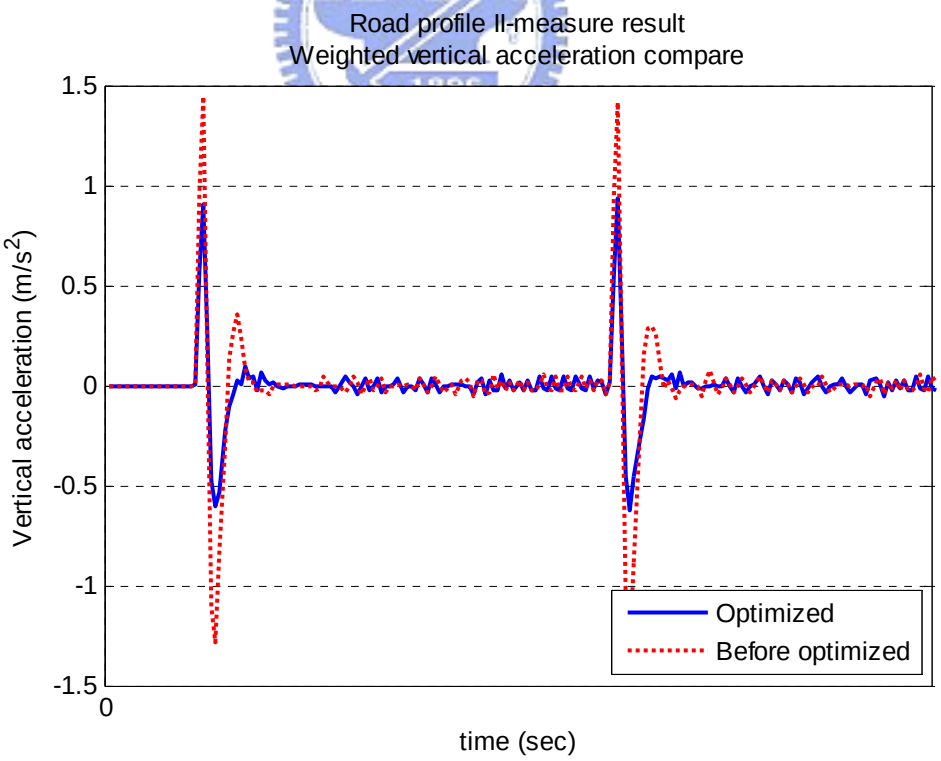

Figure 4.26 Road profile II-measure result, weighted vertical acceleration compare between 0 and 6 sec.

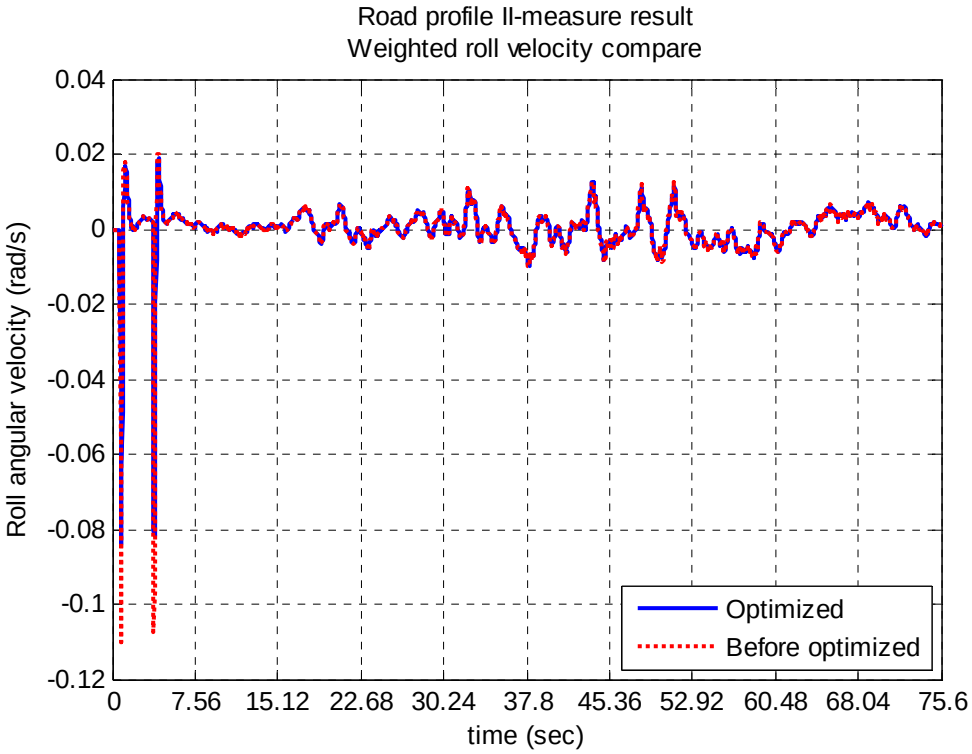

Figure 4.27 Road profile II-measure result, weighted roll velocity compare.

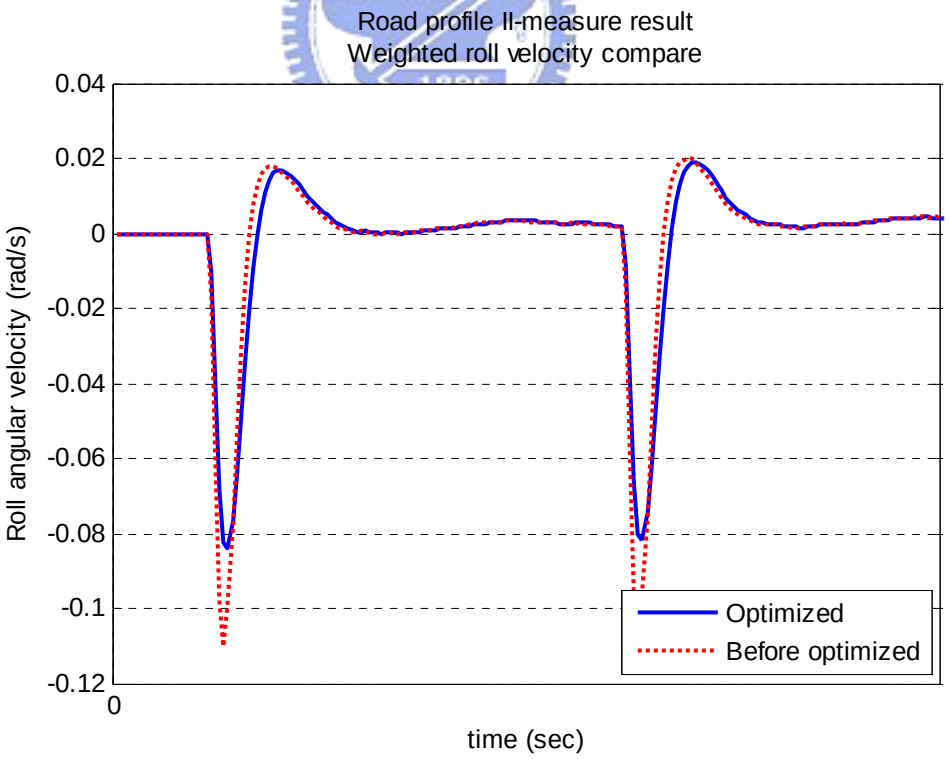

Figure 4.28 Road profile II-measure result, weighted roll velocity compare between 0 and 6 sec.

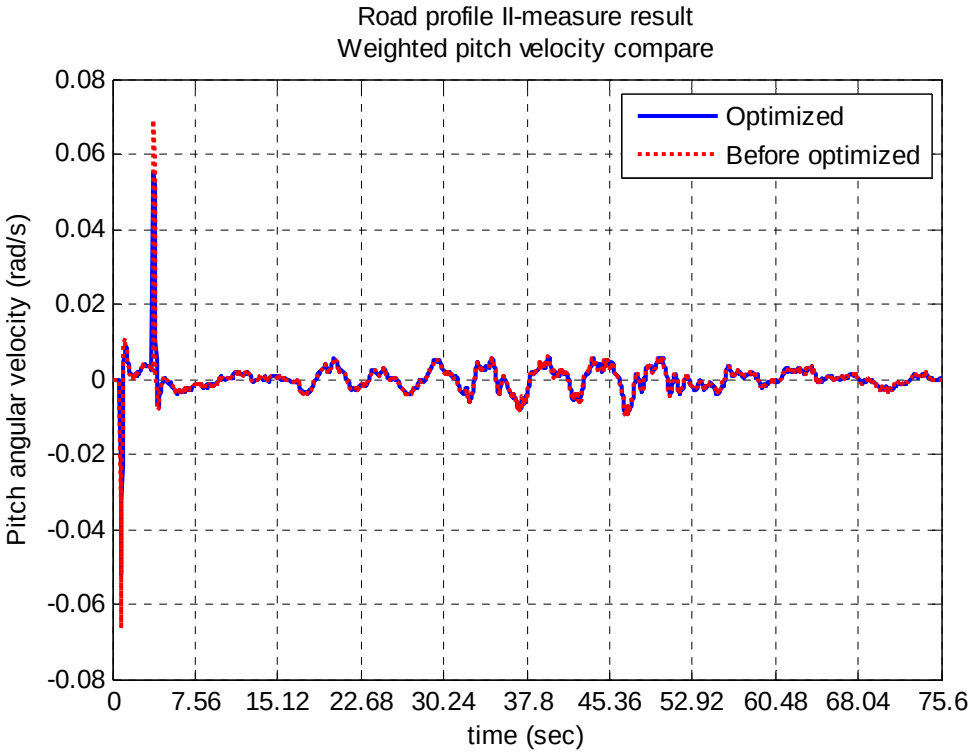

Figure 4.29 Road profile II-measure result, weighted pitch velocity compare.

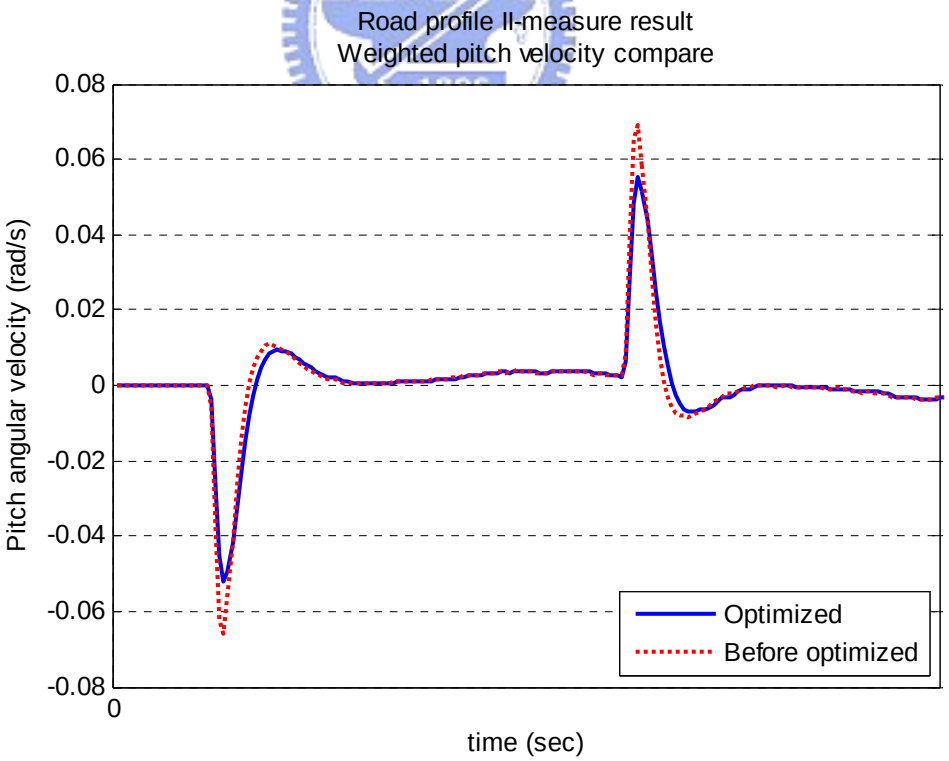

Figure 4.30 Road profile II-measure result, weighted pitch velocity compare between 0 and 6 sec

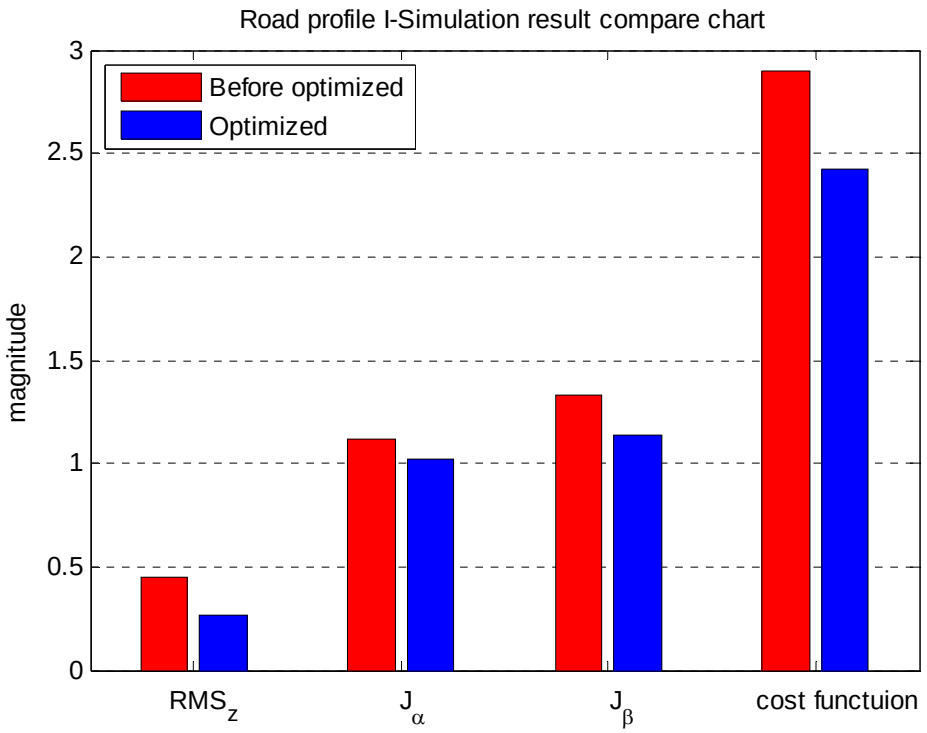

Figure 4.31 Road profile I-the simulation results compare chart.

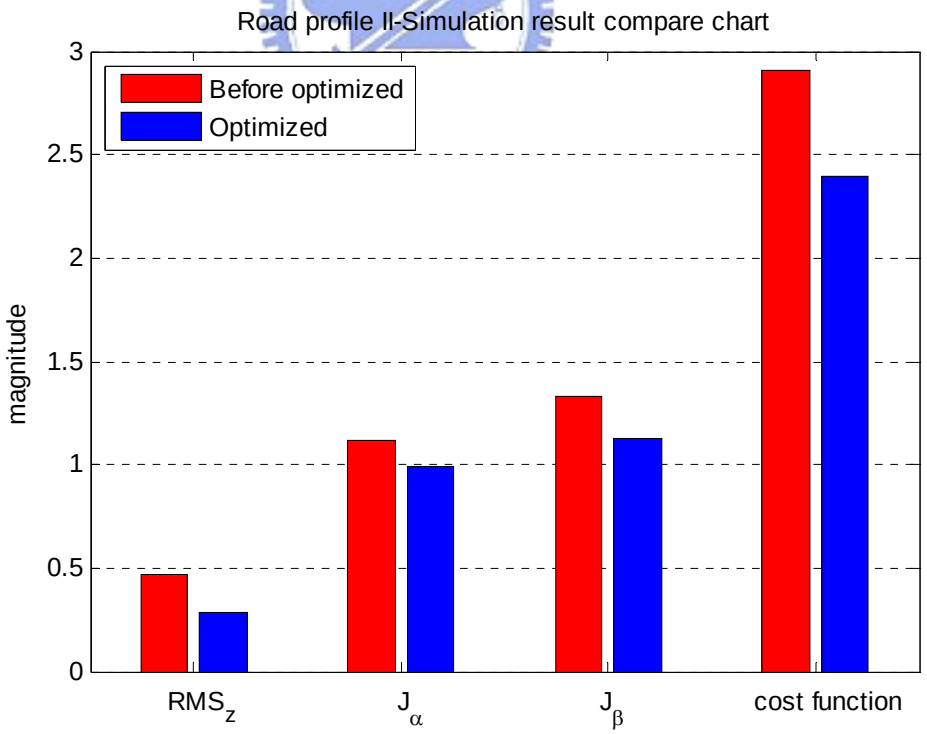

Figure 4.32 Road profile II-the simulation results compare chart.

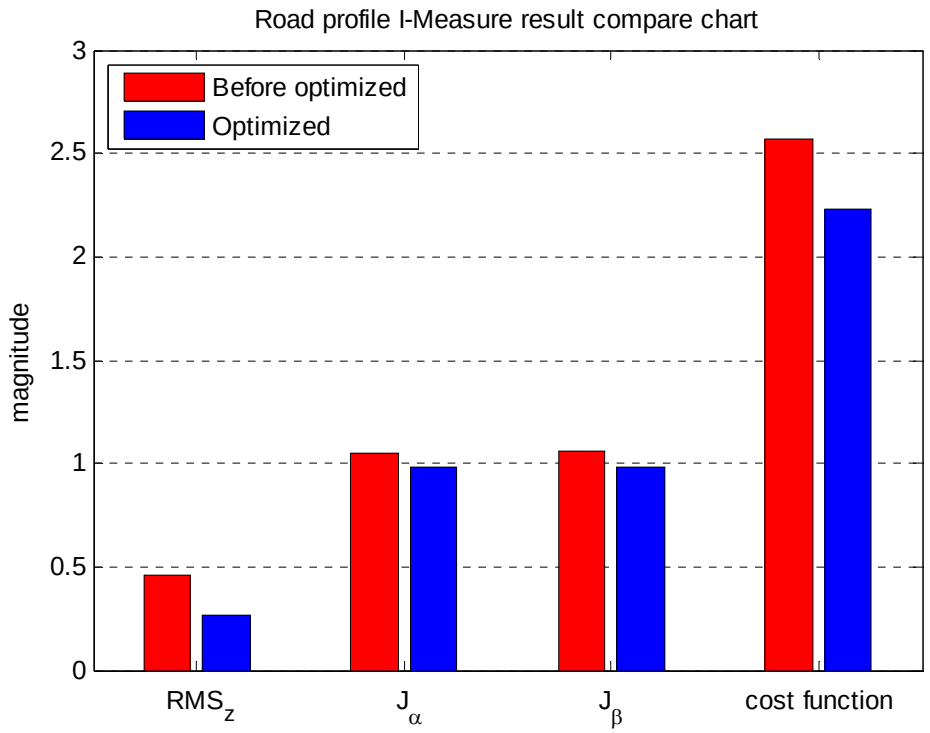

Figure 4.33 Road profile I-the measure results compare chart.

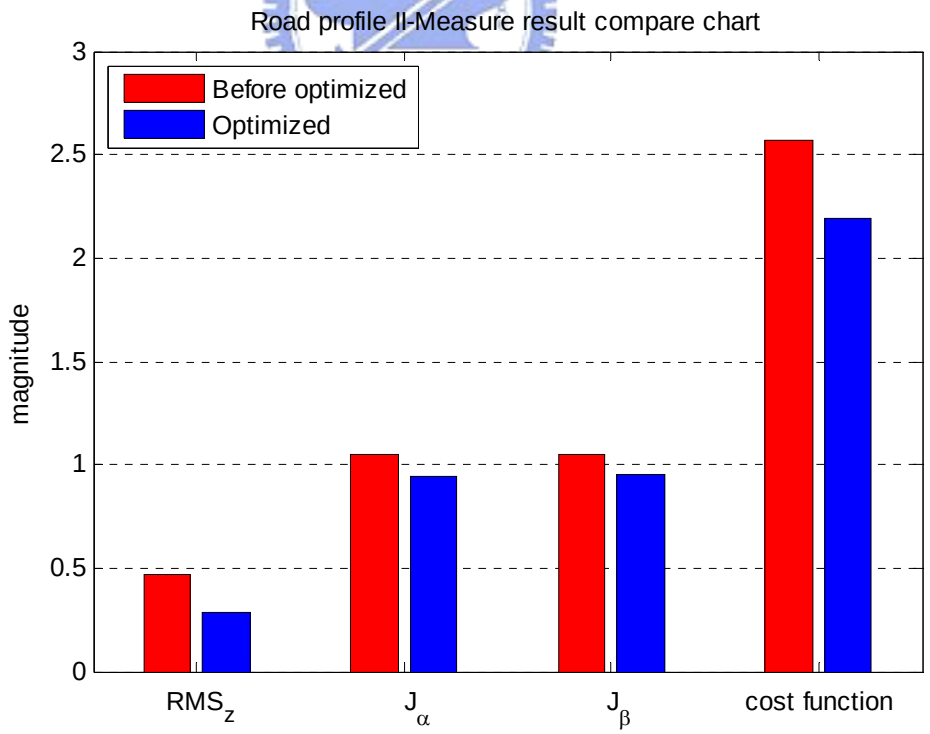

Figure 4.34 Road profile II-the measure results compare chart.

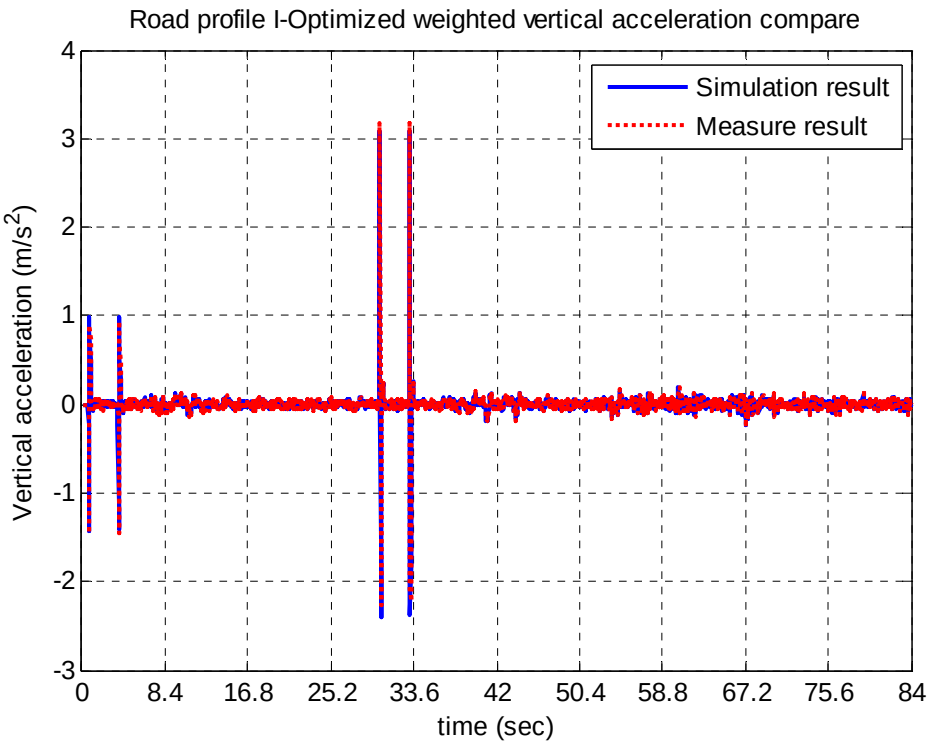

Figure 4.35 Road profile I-Optimized weighted vertical acceleration compare.

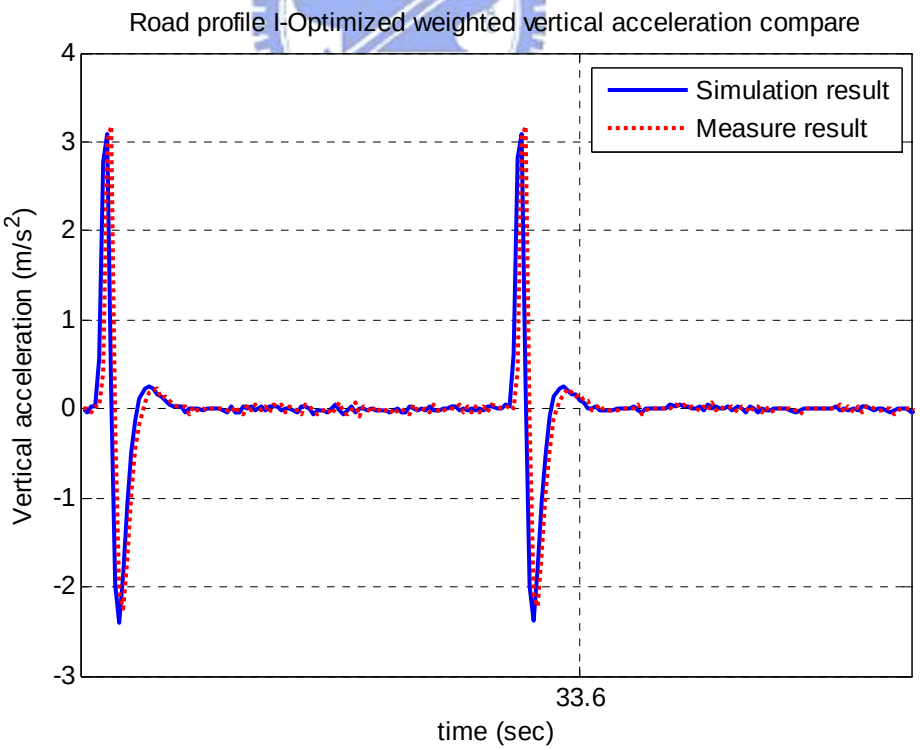

Figure 4.36 Road profile I-Optimized weighted vertical acceleration compare between 30 and 36 sec.

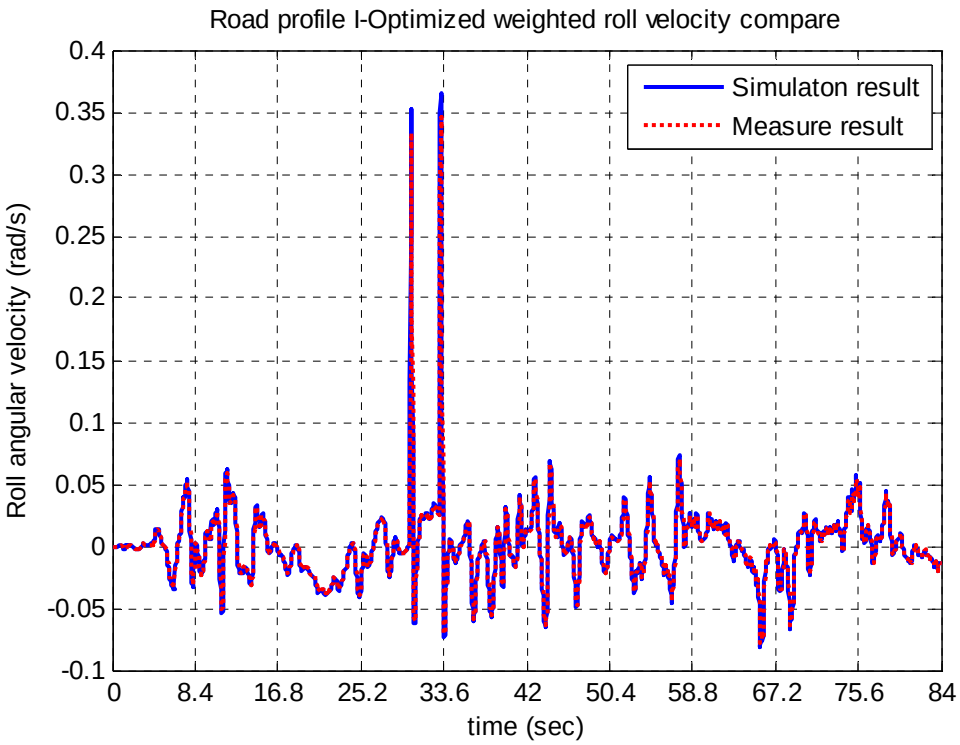

Figure 4.37 Road profile I-Optimized weighted roll velocity compare.

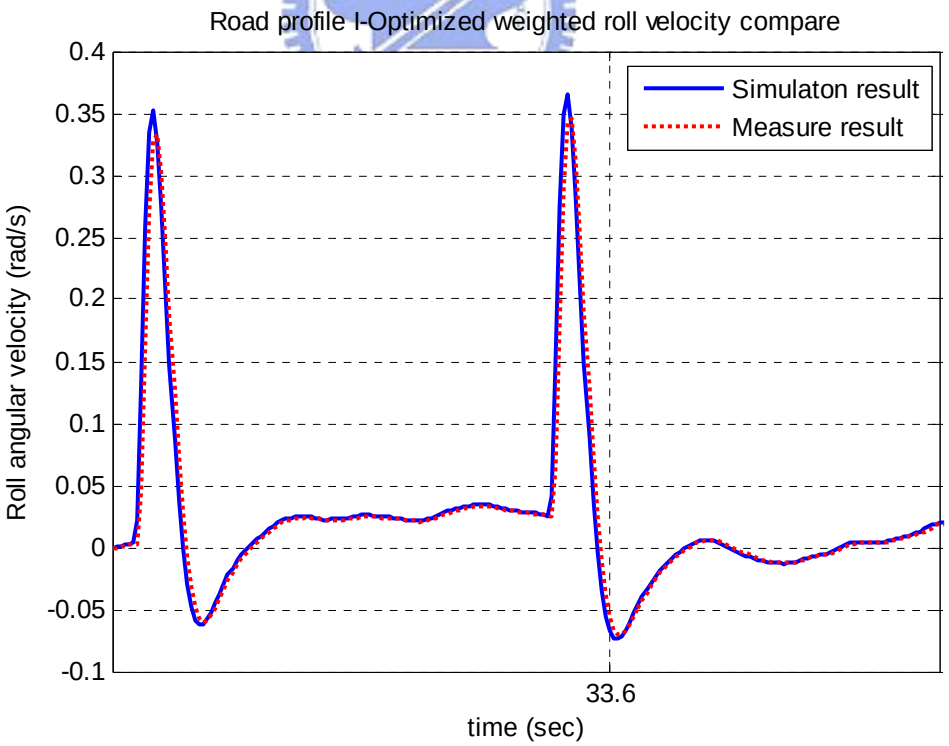

Figure 4.38 Road profile I-Optimized weighted roll velocity compare between 30 and 36 sec.

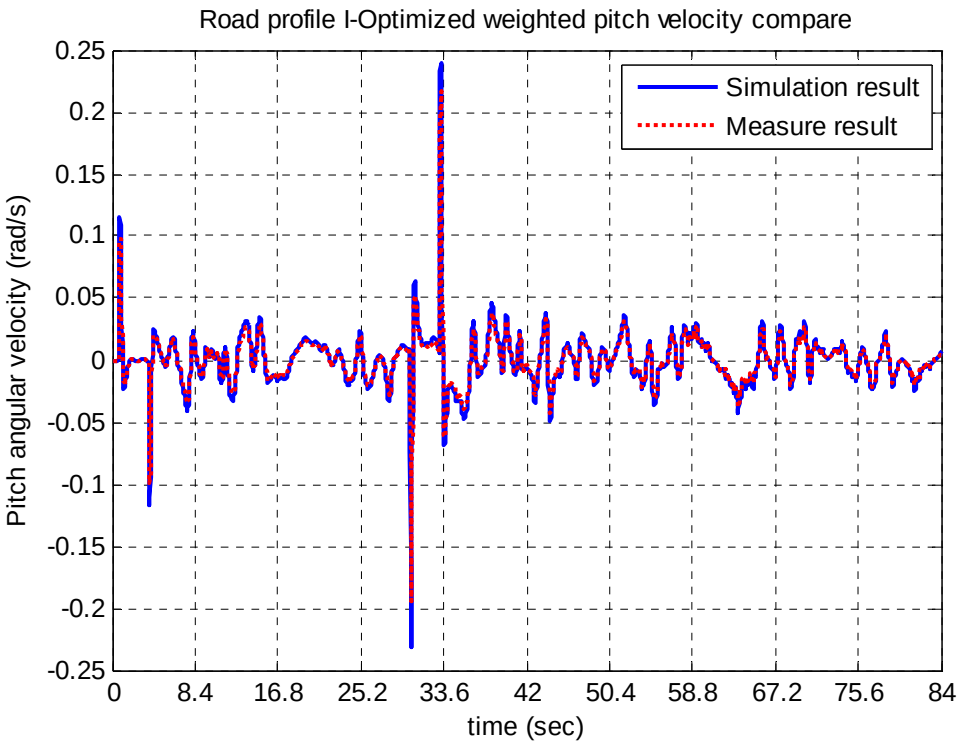

Figure 4.39 Road profile I-Optimized weighted pitch velocity compare.

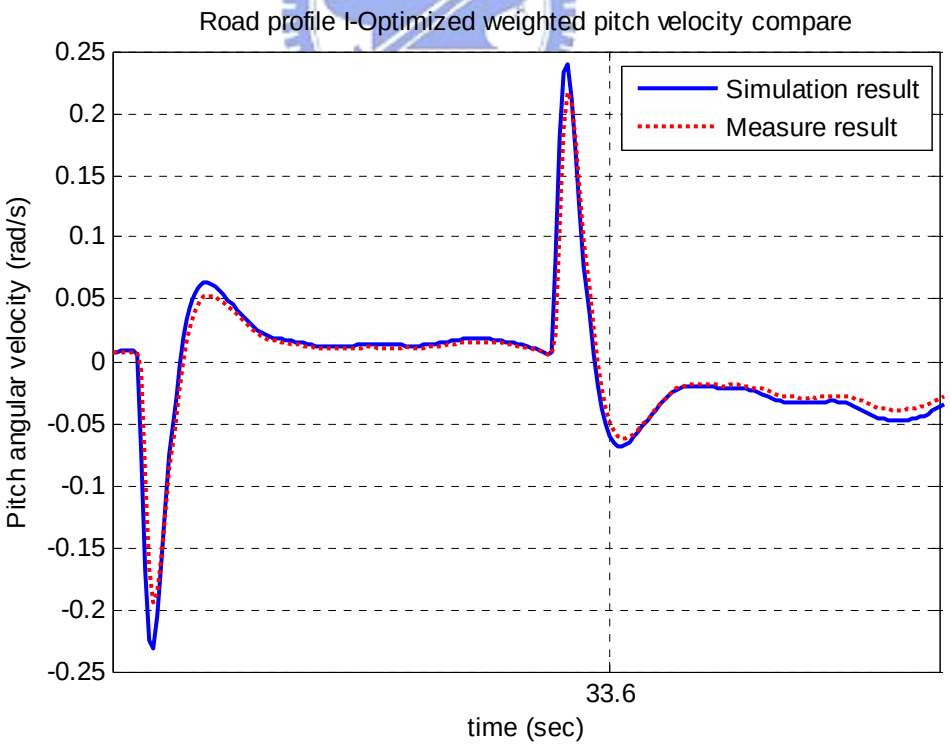

Figure 4.40 Road profile I-Optimized weighted pitch velocity compare between 30 and 36 sec.

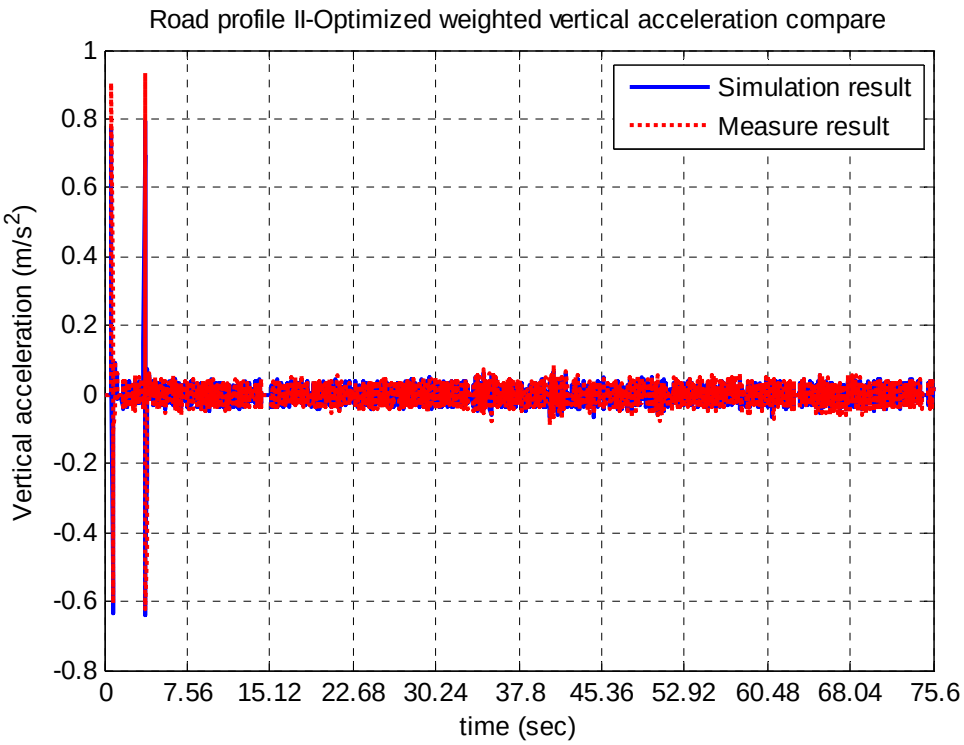

Figure 4.41 Road profile II-Optimized weighted vertical acceleration compare.

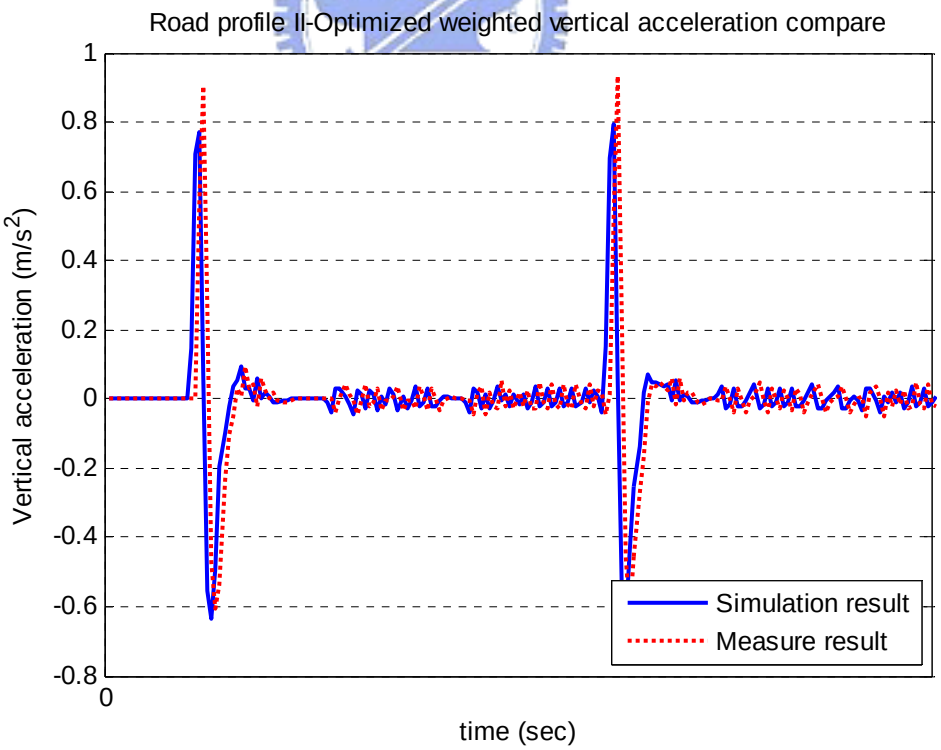

Figure 4.42 Road profile II-Optimized weighted vertical acceleration compare between 0 and 6 sec.

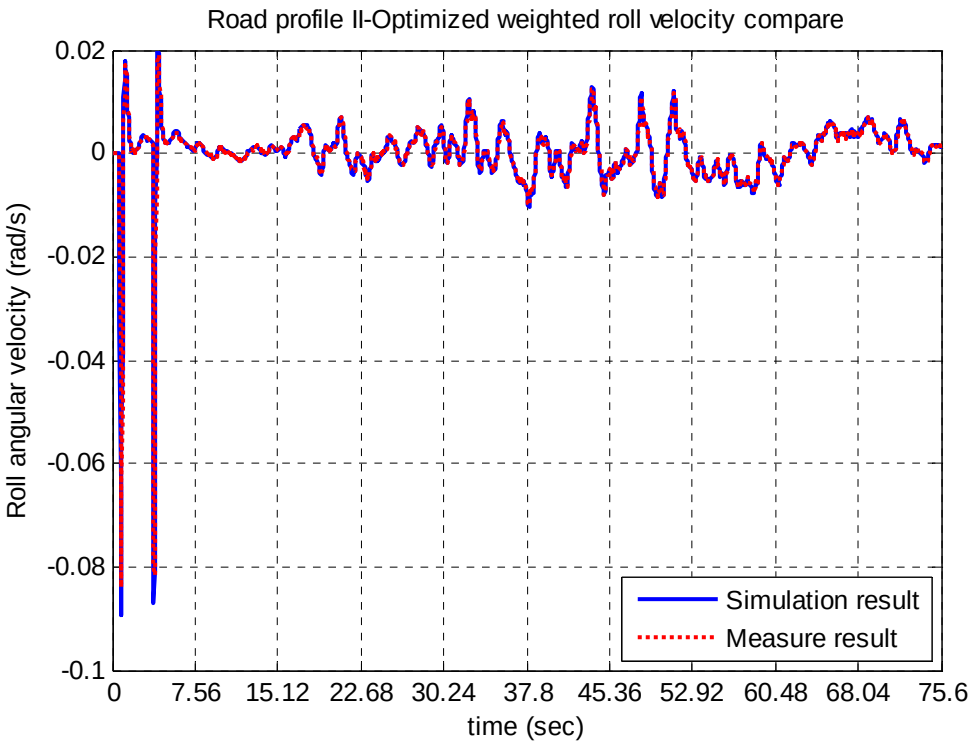

Figure 4.43 Road profile II-Optimized weighted roll velocity compare.

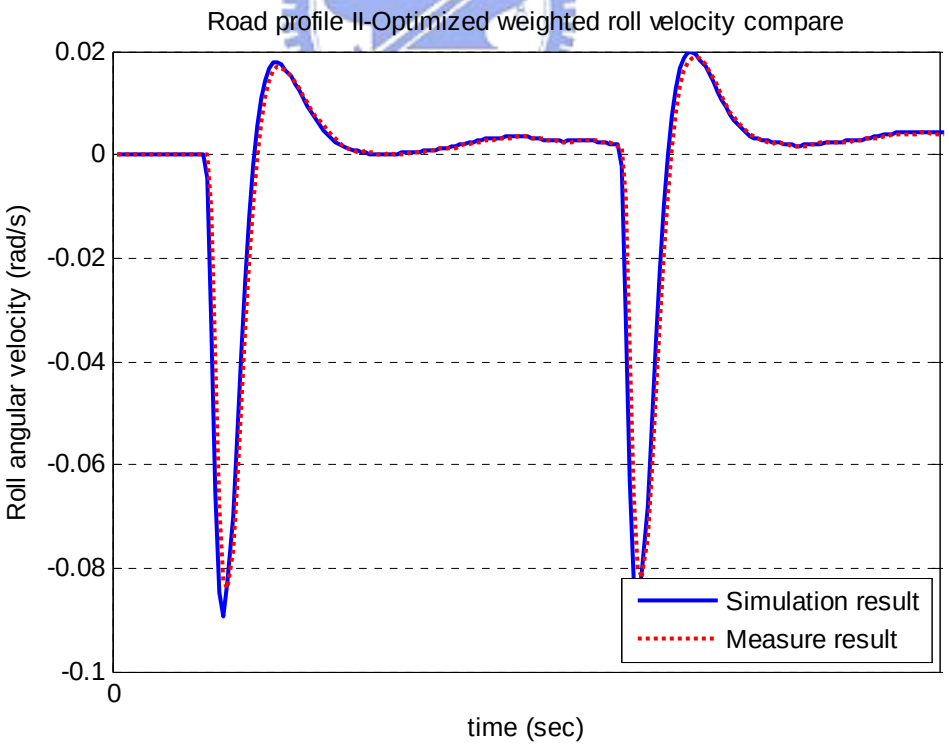

Figure 4.44 Road profile II-Optimized weighted roll velocity compare between 0 and 6 sec.

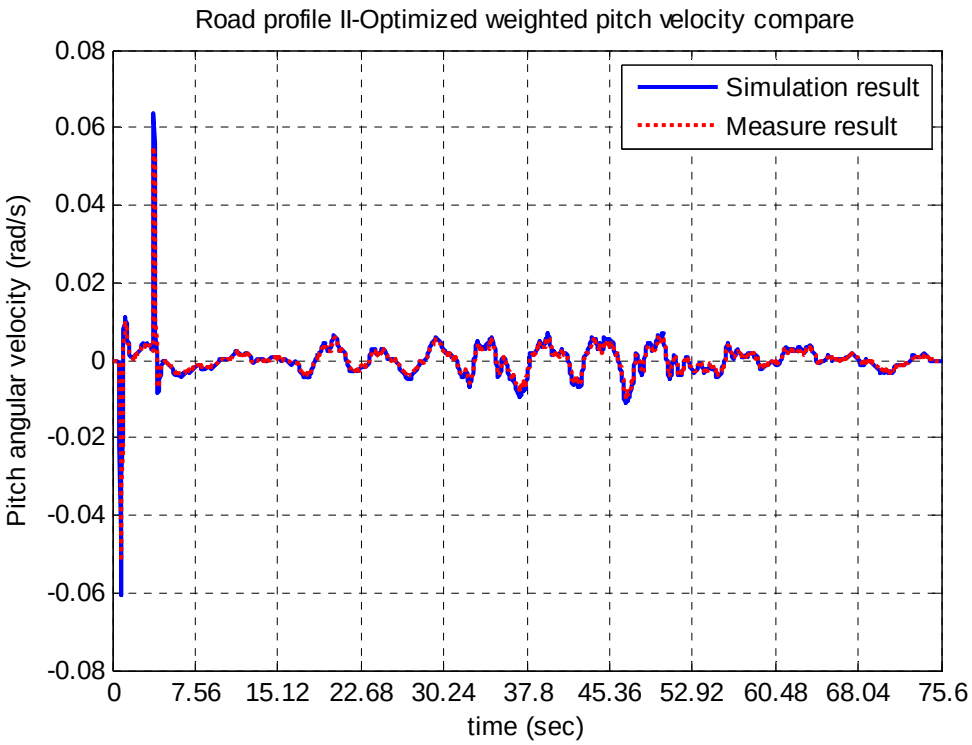

Figure 4.45 Road profile II-Optimized weighted pitch velocity compare.

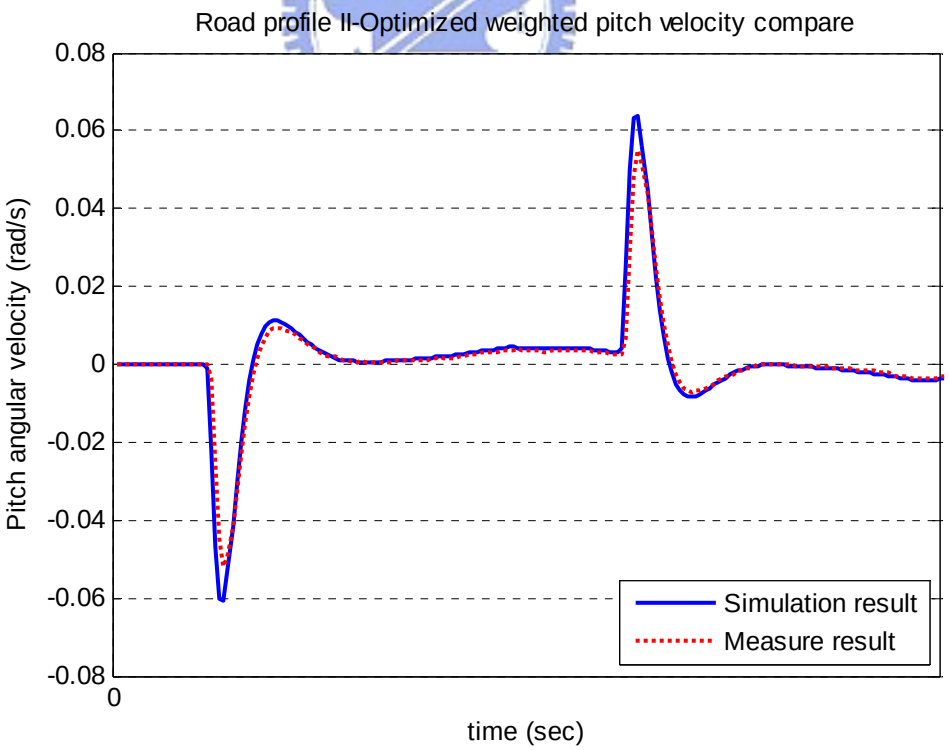

Figure 4.46 Road profile II-Optimized weighted pitch velocity compare between 0 and 6 sec.